



# Cardinal Buoys: An Opportunity for the Study of Air-Sea CO<sub>2</sub> Fluxes in Coastal Ecosystems

Jean-Philippe Gac, Pierre Marrec, Thierry Cariou, Christophe Guillerm, Éric Macé, Marc Vernet, Yann Bozec

## ► To cite this version:

Jean-Philippe Gac, Pierre Marrec, Thierry Cariou, Christophe Guillerm, Éric Macé, et al.. Cardinal Buoys: An Opportunity for the Study of Air-Sea CO<sub>2</sub> Fluxes in Coastal Ecosystems. *Frontiers in Marine Science*, 2020, 7, 10.3389/fmars.2020.00712 . hal-02944673

**HAL Id: hal-02944673**

**<https://hal.sorbonne-universite.fr/hal-02944673>**

Submitted on 21 Sep 2020

**HAL** is a multi-disciplinary open access archive for the deposit and dissemination of scientific research documents, whether they are published or not. The documents may come from teaching and research institutions in France or abroad, or from public or private research centers.

L'archive ouverte pluridisciplinaire **HAL**, est destinée au dépôt et à la diffusion de documents scientifiques de niveau recherche, publiés ou non, émanant des établissements d'enseignement et de recherche français ou étrangers, des laboratoires publics ou privés.



# Cardinal Buoys: An Opportunity for the Study of Air-Sea CO<sub>2</sub> Fluxes in Coastal Ecosystems

Jean-Philippe Gac<sup>1</sup>, Pierre Marrec<sup>2</sup>, Thierry Cariou<sup>1</sup>, Christophe Guillerm<sup>3</sup>, Éric Macé<sup>1</sup>, Marc Vernet<sup>1</sup> and Yann Bozec<sup>1\*</sup>

<sup>1</sup> CNRS, Sorbonne Université, UMR 7144 AD2M, Station Biologique de Roscoff, Roscoff, France, <sup>2</sup> Graduate School of Oceanography, University of Rhode Island, Narragansett, RI, United States, <sup>3</sup> Division Technique INSU/CNRS, Technopôle Brest Iroise, Plouzané, France

## OPEN ACCESS

### Edited by:

Masao Ishii,  
Meteorological Research Institute  
(MRI), Japan

### Reviewed by:

Adrienne J. Sutton,  
Pacific Marine Environmental  
Laboratory (NOAA), United States  
Shinya Kouketsu,  
Japan Agency for Marine-Earth  
Science and Technology (JAMSTEC),  
Japan

### \*Correspondence:

Yann Bozec  
bozec@sb-roscoff.fr

### Specialty section:

This article was submitted to  
Ocean Observation,  
a section of the journal  
Frontiers in Marine Science

**Received:** 22 May 2020

**Accepted:** 04 August 2020

**Published:** 31 August 2020

### Citation:

Gac J-P, Marrec P, Cariou T,  
Guillerm C, Macé É, Vernet M and  
Bozec Y (2020) Cardinal Buoys: An  
Opportunity for the Study of Air-Sea  
CO<sub>2</sub> Fluxes in Coastal Ecosystems.  
Front. Mar. Sci. 7:712.  
doi: 10.3389/fmars.2020.00712

From 2015 to 2019 we installed high-frequency (HF) sea surface temperature (SST), salinity, fluorescence, dissolved oxygen (DO) and partial pressure of CO<sub>2</sub> (pCO<sub>2</sub>) sensors on a cardinal buoy of opportunity (ASTAN) at a coastal site in the southern Western English Channel (sWEC) highly influenced by tidal cycles. The sensors were calibrated against bimonthly discrete measurements performed at two long-term time series stations near the buoy, thus providing a robust multi-annual HF dataset. The tidal transport of a previously unidentified coastal water mass and an offshore water mass strongly impacted the daily and seasonal variability of pCO<sub>2</sub> and pH. The maximum tidal variability associated to spring tides (>7 m) during phytoplankton blooms represented up to 40% of the pCO<sub>2</sub> annual signal at ASTAN. At the same time, the daily variability of 0.12 pH units associated to this tidal transport was 6 times larger than the annual acidification trend observed in the area. A frequency/time analysis of the HF signal revealed the presence of a day/night cycle in the tidal signal. The diel biological cycle accounted for 9% of the annual pCO<sub>2</sub> amplitude during spring phytoplankton blooms. The duration and intensity of the biologically productive periods, characterized by large inter-annual variability, were the main drivers of pCO<sub>2</sub> dynamics. HF monitoring enabled us to accurately constrain, for the first-time, annual estimates of air-sea CO<sub>2</sub> exchanges in the nearshore tidally-influenced waters of the sWEC, which were a weak source to the atmosphere at 0.51 mol CO<sub>2</sub> m<sup>-2</sup> yr<sup>-1</sup>. This estimate, combined with previous studies, provided a full latitudinal representation of the WEC (from 48°75' N to 50°25' N) over multiple years for air-sea CO<sub>2</sub> fluxes in contrasted coastal ecosystems. The latitudinal comparison showed a clear gradient from a weak source of CO<sub>2</sub> in the tidal mixing region toward sinks of CO<sub>2</sub> in the stratified region with a seasonal thermal front separating these hydrographical provinces. In view of the fact that several continental shelf regions have been reported to have switched from sources to sinks of CO<sub>2</sub> in the last century, weak CO<sub>2</sub> sources in such tidal mixing areas could potentially become sinks of atmospheric CO<sub>2</sub> in coming decades.

**Keywords:** buoy of opportunity, high-frequency, tidal cycle, multi-annual, air-sea CO<sub>2</sub> exchanges, ocean acidification, coastal ecosystems

## INTRODUCTION

The dynamics of the carbonate system in the ocean are complex and simultaneously controlled by physical, chemical, and biological processes (Zeebe and Wolf-Gladrow, 2001). As an interface between land, ocean, and atmosphere, coastal ecosystems are characterized by strong physical and biogeochemical heterogeneity, introducing further complexity into the coastal carbon cycle and carbonate system dynamics (Walsh, 1991; Gattuso et al., 1998; Muller-Karger et al., 2005). Despite representing only 7% of the global ocean, coastal ecosystems are a key component of the global carbon cycle because of their disproportionately high rates of primary production (10–30%) and organic matter remineralization (Walsh et al., 1988; de Haas et al., 2002; Bauer et al., 2013). The coastal ocean therefore exhibits enhanced air-sea CO<sub>2</sub> fluxes (FCO<sub>2</sub>) compared to open oceans (Tsunogai et al., 1999; Thomas et al., 2004; Chen and Borges, 2009). According to the most recent estimates, during the 1998–2015 period coastal ecosystems were a global CO<sub>2</sub> sink of  $0.20 \pm 0.02 \text{ Pg C yr}^{-1}$  compared to a net CO<sub>2</sub> sink of  $1.7 \pm 0.3 \text{ Pg C yr}^{-1}$  for the open ocean (Roobaert et al., 2019). Coastal ecosystems account for 13% of the total CO<sub>2</sub> sink despite representing a much lower proportion of global ocean surface area (7%). In terms of anthropogenic CO<sub>2</sub> sink, coastal ecosystems represent 4.5% (Bourgeois et al., 2016) of the latest estimates of  $2.6 \pm 0.3 \text{ Pg C yr}^{-1}$  for the 1994–2007 period (Gruber et al., 2019) and  $2.6 \pm 0.6 \text{ Pg C yr}^{-1}$  for the last decade (Friedlingstein et al., 2019). Due to their proximity with human activities, coastal ecosystems are also particularly vulnerable to anthropogenic forcing such as eutrophication and ocean acidification (OA) (Borges and Gypens, 2010; Borges et al., 2010; Cai et al., 2011, 2017; Bauer et al., 2013). Coastal ecosystems can show extremes of OA hotspots due to the intrusion of acidified water with low saturation state  $\Omega_{\text{arag}}$  (Feely et al., 2016, 2010; Chan et al., 2017; Fennel et al., 2019) or conversely constitute refuge with more stable pH (Chan et al., 2017).

In the context of climate change and continuous atmospheric CO<sub>2</sub> increase, unraveling CO<sub>2</sub> system dynamics and air-sea CO<sub>2</sub> fluxes in coastal ecosystems remains a major challenge (Laruelle et al., 2018). Long-term high-frequency (HF) monitoring of the carbonate system in coastal ecosystems is essential to distinguish natural variability from responses to anthropogenically induced changes at various temporal and spatial scales (Borges et al., 2010; Ciais et al., 2014). Extreme or short-scale events may affect mean estimates of coastal carbon fluxes, thus budgets based on short time-series of observations should seldom be viewed with caution (Salisbury et al., 2009). In the past decade, autonomous moorings and observing platforms considerably improved estimates of air-sea CO<sub>2</sub> fluxes at various time and spatial scales to better constrain carbon budgets in coastal ecosystems (Sutton et al., 2014; Xue et al., 2016; Reimer et al., 2017). Recent technical advances in terms of measurement of partial pressure of surface CO<sub>2</sub> (pCO<sub>2</sub>) and pH (Sastri et al., 2019) mean that it is now possible to develop accurate long-term records of these parameters in nearshore ecosystems. Combining HF measurements of pH or pCO<sub>2</sub> with discrete carbonate system parameters (DIC/TA) can be a valuable tool for carbon cycle

research based on autonomous moorings (Cullison Gray et al., 2011). This type of calibrated data could then potentially be included in large international databases such as the Surface Ocean CO<sub>2</sub> Atlas (SOCAT, Bakker et al., 2016).

A key challenge for the scientific community focusing on the coastal marine environment is to integrate observations of essential ocean variables for physical, biogeochemical, and biological processes on appropriate spatial and temporal scales, in a sustained and scientifically based manner (Farcy et al., 2019). The European projects JERICO and JERICO-Next (2010–2020) built an integrated and innovation-driven coastal research infrastructure for Europe, notably for the observation of the carbonate system parameters, based on Voluntary Observation Ships (VOS), long-term time series, and buoys of opportunity (Puillat et al., 2016; Farcy et al., 2019). From 2011 to 2015, a VOS program provided seasonal and latitudinal HF measurements across the Western English Channel (WEC), enabling first assessments of air-sea CO<sub>2</sub> fluxes (FCO<sub>2</sub>) dynamics in the WEC and adjacent coastal seas (Marrec et al., 2013, 2014, 2015). As part of the French network for the monitoring of coastal environments (SOMLIT<sup>1</sup>), two long-term time-series in the WEC off Roscoff have been implemented to monitor carbonate parameters at SOMLIT-pier and SOMLIT-offshore stations. Sampling in this program is bimonthly and can therefore miss specific, short-term events occurring between scheduled sampling dates. In the framework of the national program COAST-HF (Coastal Ocean Observing System-High Frequency<sup>2</sup>), the cardinal buoy of opportunity “ASTAN,” located halfway between the two SOMLIT sampling sites, was equipped with oceanographic and meteorological sensors to complete the discrete sampling.

This study describes the benefits and challenges of deploying and maintaining a HF autonomous coastal observation platform of opportunity. We report the results of 5 years of HF pCO<sub>2</sub> and ancillary data recorded at the ASTAN buoy and 5 years of low frequency monitoring of similar parameters at the SOMLIT-pier and SOMLIT-offshore sites. We examine the dynamics of sea surface pCO<sub>2</sub> and associated FCO<sub>2</sub> from tidal to inter-annual timescales. We identify the main factors controlling pCO<sub>2</sub> variability at short timescales using frequency analysis and quantify the impact of the tidal and diel cycles on CO<sub>2</sub> system dynamics. Ultimately, we place the annual FCO<sub>2</sub> data in a broader context to fully describe the latitudinal variability of FCO<sub>2</sub> throughout the WEC.

## STUDY SITE

The WEC is part of the North-West European continental shelf, one of the world's largest temperate margins, and is a pathway between the North Atlantic and the North Sea. High salinity and relatively warm waters from the North Atlantic Drift flow eastward to the western Channel entrance (Salomon and Breton, 1993). The WEC is characterized by three distinct hydrographical

<sup>1</sup><http://somalit.epoc.u-bordeaux1.fr/>

<sup>2</sup><http://coast-hf.fr>

regimes: permanently well-mixed waters in the southern WEC (sWEC), seasonally stratified waters in the northern WEC (nWEC) and a frontal structure separating these hydrographical provinces (Pingree and Griffiths, 1978). The intense tidal streams permanently mix the water column from the bottom to the surface all year round in the sWEC, although weak and brief stratification can occur during summer, particularly during neap tides with low wind velocity (L'Helguen et al., 1996; Guilloux et al., 2013). Many rivers and estuaries discharge freshwater into the sWEC, with enhanced river influx during winter due to intense precipitation (Tréguer et al., 2014). These freshwater inputs release nutrient stocks into the marine environment (Meybeck et al., 2006; Dürr et al., 2011; Tréguer and De La Rocha, 2013) fueling spring phytoplankton blooms (e.g., Del Amo et al., 1997; Beucher et al., 2004) and maintaining substantial primary productivity in summer, when light is the limiting factor, not nutrients (Wafar et al., 1983).

The ASTAN buoy is a cardinal buoy of opportunity located 3.1 km offshore from Roscoff (48°44'55" N; 3°57'40" W, **Figure 1**), east of the Batz Island. The mean bathymetry is around 45 m. This location is characterized by strong tidal streams with a tidal range up to 8 m during spring tides. The weather conditions can be rough with frequent gusts of wind and storms making work at sea difficult, especially on a mooring. During winter storms, the swell and waves north of the Batz Island can reach 6–7 m high, but the mooring is somewhat protected by the island from swell from the North Atlantic Ocean.

Two low-frequency stations are present either side of the HF buoy (**Figure 1**), with SOMLIT-pier located south of the buoy (48°43'59" N; 3°58'58" W) and SOMLIT-offshore located north (48°46'49" N; 3°58'14" W). Despite their close proximity, these two stations are quite different. SOMLIT-pier is located very close to the coast, strongly influenced by coastal waters, with a particular hydrodynamic regime: a strong tidal range and a low water column (around 5 m). SOMLIT-offshore is characteristic of sWEC surface waters with a well-mixed water column (around 60 m), with the distance from the coast (3.5 km) limiting the impact of rainwater and river inflow.

## MATERIALS AND METHODS

### High-Frequency Measurements From the ASTAN Buoy

From 2015 to 2019, conductivity and temperature were recorded every 30 min using a SBE16 + (SeaBird, Inc.) instrument. A Cyclops7 fluorimeter (Turner Designs, Inc.) and a SBE43 sensor (SeaBird, Inc.) measured at the same frequency Chl-*a* fluorescence and DO, respectively. The manufacturer accuracies were  $\pm 0.005^\circ\text{C}$  for the temperature sensor, 2% for oxygen saturation and 0.0005 S/m for conductivity. TBTO® anti-fouling cylinders and black Tygon® tubing were installed in the pumping circuit to prevent biofouling, which is a major issue for deployment of sensors in coastal water, with a critical period from May to September.

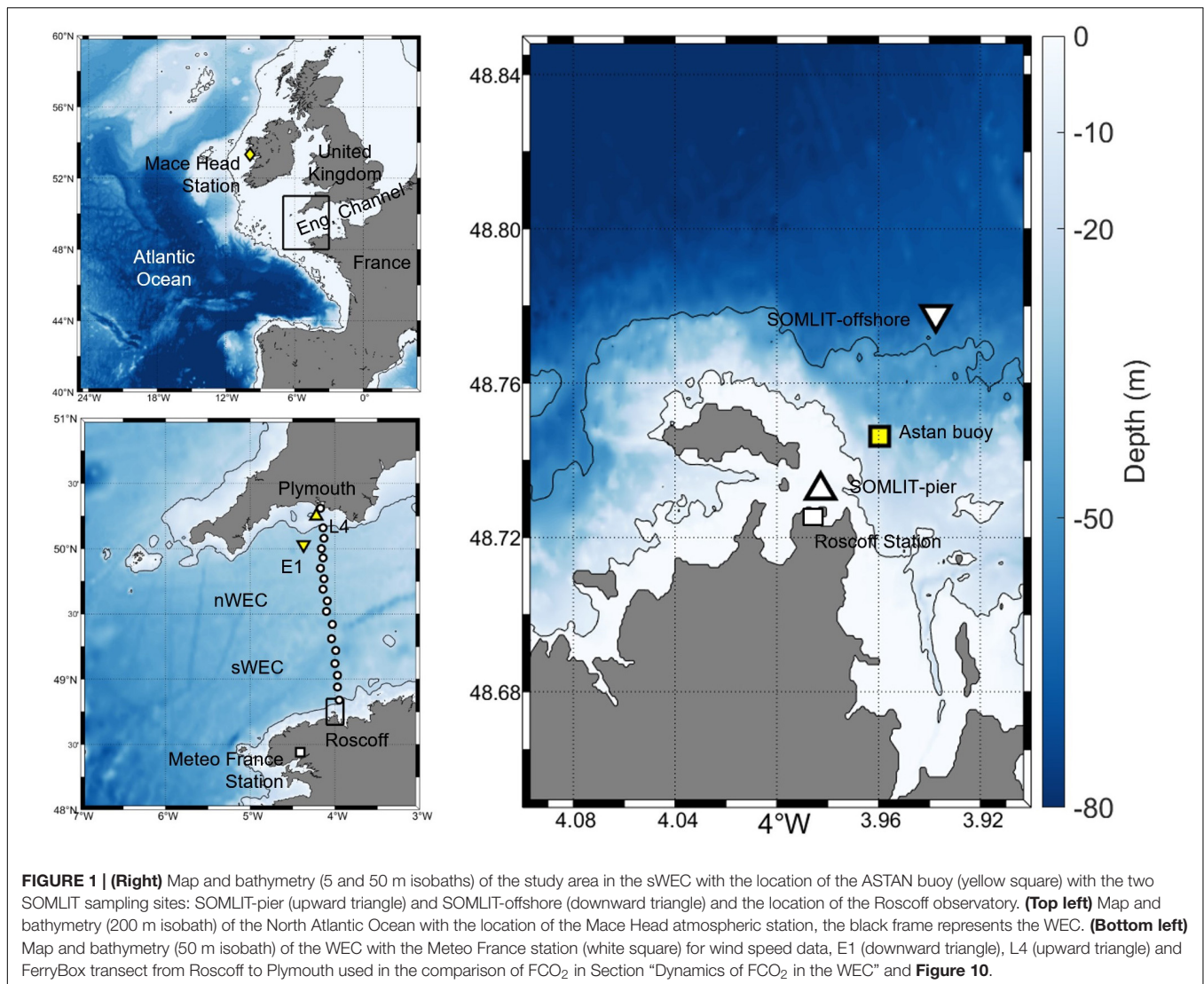
A Submersible Autonomous Moored Instrument for CO<sub>2</sub> (SAMI-CO<sub>2</sub>, SunBurst Sensors) was installed from March 2015

to December 2019 to measure pCO<sub>2</sub> in seawater with a 1-h frequency. The SAMI-CO<sub>2</sub> sensor uses calibrated reagent-based colorimetry to measure the change in pH of the dye [bromothymol blue (BTB)]. The BTB is contained in a gas-permeable membrane that is exposed to the environment. The pH change is driven by diffusion of CO<sub>2</sub> across the membrane. The dye absorbance is recorded at two wavelengths, corresponding to the absorption peaks of acid/base forms of BTB. Blank measurements were performed regularly in distilled water for quality control. The accuracy of measurements reported by the manufacturer is  $\pm 8 \mu\text{atm}$  (DeGrandpre et al., 1997). All sensors were recovered every 3 months for inspection, cleaning, battery checks and control of reagent levels.

### Bimonthly Measurements at Fixed Stations SOMLIT-Pier and SOMLIT-Offshore

From March 2015 to December 2019, bimonthly sampling was performed at SOMLIT-pier and SOMLIT-offshore fixed stations (**Figure 1**) during neap tides and at high tide slack. CTD profiles were obtained with a Seabird SBE19 + with accuracies for temperature and computed salinity of 0.005°C and 0.002 respectively. Discrete seawater was sampled using 10 L Niskin bottle. Salinity measurements were performed by sampling seawater in glass bottles with a rubber seal and analyzed in the following months in a temperature regulated room with a portasal Guidline Salinometer at the SHOM (Service Hydrographique et Oceanographique de la Marine) with an accuracy of 0.002. For DO measurements seawater from the Niskin bottle was transferred into 280 mL brown glass bottles that were sealed with special caps to remove all air after addition of 1.7 mL of Winkler reagent I and II. Bottles were kept in the dark in a water bath and analyzed by the Winkler method using potentiometric end-point determination using a Metrohm titrator. The estimated accuracy of this method is 0.2  $\mu\text{M}$  (Carpenter, 1965). For Chl-*a* measurements 500 ml of seawater were filtered through a GF/F (Whatman) glass filter under 0.2 bar vacuum. The filters were stored in a plastic tube at  $-20^\circ\text{C}$  before analysis. The EPA (1997) extraction method was used in which Chl-*a* was extracted in a 90% acetone solution for a few hours at 4°C, followed by measurement of Chl-*a* concentration using a Turner AU10 fluorometer. Nutrient concentrations ( $\text{PO}_4^{3-}$  and  $\text{SiO}_4^{2-}$ ) were determined using an AA3 auto-analyzer (AXFLOW) following the method of Aminot and Kérouel (2007) with accuracies of 1 ng L<sup>-1</sup> and 0.01  $\mu\text{g L}^{-1}$  for  $\text{PO}_4^{3-}$  and  $\text{SiO}_4^{2-}$ , respectively. During the same period, total alkalinity (TA), dissolved inorganic carbon (DIC) and pH were measured at SOMLIT-pier and SOMLIT-offshore stations. Seawater was sampled in 500 mL borosilicate glass bottles and poisoned with 50  $\mu\text{L}$  of saturated HgCl<sub>2</sub>. TA and the DIC were determined at the SNAPO (Service National d'Analyse des Paramètres Océaniques) using potentiometric analysis following the Edmond (1970) method and DOE (1994) with accuracies of 2.5  $\mu\text{mol kg}^{-1}$  for both parameters (see Marrec et al., 2013 for details on this method). pH was determined using the same protocol as for the ASTAN buoy measurements (see below).





From March 2017 to December 2019, additional sampling for pH and TA in the vicinity of the ASTAN buoy was performed every 2 weeks. 50 discrete samples for the determination of TA and pH were collected in 500 mL borosilicate glass bottles and poisoned with 50  $\mu\text{L}$  of saturated  $\text{HgCl}_2$ . TA was determined from approximately 51 g of weighed sample at 25°C using a potentiometric titration with 0.1M HCl using a Titrino 847 plus Metrohm. The balance point was determined by the Gran method (Gran, 1952) according to the method of Haraldsson et al. (1997). The accuracy of this method is  $\pm 2.1 \mu\text{mol kg}^{-1}$  (Millero, 2007) and was verified by Certified Reference Material (CRM 131) provided by A. Dickson (Scripps Institute of Oceanography, University of South California, San Diego, United States). pH was determined with an accuracy of 0.002 pH units by spectrophotometry (Perin-Elmer Lambda 11) at a controlled temperature of 25°C with the method of Clayton and Byrne (1993) and corrected by Chierici et al. (1999), using the sulfonephthaleindiprotic indicator of meta-CresolPurple (mCP).

## Calculated Data

### Dissolved Oxygen Saturation

Calculation of dissolved oxygen saturation (DO%) gives access to the impact of non-thermodynamical processes, such as biological production and respiration, on the variation of DO. The DO% was calculated from Eq. 1 using *in situ* temperature, salinity, and dissolved oxygen concentrations.

$$\begin{aligned} \ln C^* &= A_1 + \left(\frac{A_2 \times T}{100}\right) + [A_3 \times \log\left(\frac{T}{100}\right)] \\ &+ S \times [(B_1 + (B_2 \times \frac{T}{100}) + B_3 \times (\frac{T}{100})^2)] \\ DO\% &= \left(\frac{DO}{C^*}\right) \times 100 \end{aligned} \quad (1)$$

Where  $C^*$  is the concentration of DO at saturation, A and B coefficients are constants described in Weiss (1970), T is the SST (in K) and S the sea surface salinity (SSS).

## Carbonate System Parameters

At the ASTAN buoy, we used the combination of TA, pH, SSS and SST as input parameters in the CO<sub>2</sub> chemical speciation model (CO<sub>2sys</sub> Program, Pierrot et al., 2011). We used the equilibrium constants of CO<sub>2</sub> proposed by Mehrbach et al. (1973), refitted by Dickson and Millero (1987) on the total pH scale, as recommended by Dickson et al. (2007) and Orr et al. (2015), and including PO<sub>4</sub><sup>3-</sup> and SiO<sub>4</sub><sup>-</sup> concentrations. At SOMLIT-pier and SOMLIT-offshore, from January 2015 to April 2018, we used the combination of TA, DIC, SSS, SST, PO<sub>4</sub><sup>3-</sup> and SiO<sub>4</sub><sup>-</sup> concentrations, and from May 2018 to December 2019 we used the combination of pH, DIC, SSS, SST and PO<sub>4</sub><sup>3-</sup> and SiO<sub>4</sub><sup>-</sup> concentrations as input parameters in the model. We use the standard uncertainty propagation package updated by Orr et al. (2018) for comparison with current computations of uncertainty on the carbonate system parameters in the field of OA. The average uncertainty on pCO<sub>2calc</sub> were estimated at 11 μatm for TA/pH, at 18 μatm for DIC/TA and at 8 μatm for pH/DIC. These uncertainties were in agreement with similar pCO<sub>2calc</sub> computations using the propagation technique: 20 μatm for Shadwick et al. (2019) and 15 μatm for Kapsenberg et al. (2017) with DIC/TA as entry parameters.

To estimate pH variations from pCO<sub>2</sub> at the ASTAN buoy (pH<sub>calc</sub>), we relied on 20 seasonal surveys performed in 2011, 2019 and 2020, when we collected more than 150 data points for TA and SSS covering the entire SSS gradient (0–35.5) in the Penzé and Morlaix rivers, the main sources of freshwater input at our study site. We combined these data with the 2016 discrete dataset marked by intense freshwater inputs at the ASTAN site with important rainfall (563 mm during that winter compared to 274 mm during 2019), and SSS varying from 34.50 to 35.50. We were able to establish a very robust relationship between TA and SSS ( $n = 236$ ,  $r^2 = 0.98$ ) with the following equation 2 (Supplementary Figure S1):

$$TA_{calc} = 50.4(\pm 0.5) \cdot SSS + 575(\pm 14) \quad (2)$$

We therefore estimated the HF pH with CO<sub>2sys</sub> using the same parameters SST, SSS, pCO<sub>2</sub> and TA<sub>calc</sub>. We compared the discrete pH values obtained in 2019 at the ASTAN buoy with the spectrophotometric technique [precision of 0.001 and bias of 0.005 pH units (Dickson et al., 2007)] to the pH<sub>calc</sub> from the TA/SSS relationship (Supplementary Figure S2). From this comparison, we estimate the uncertainty on the pH<sub>calc</sub> at 0.04.

## Deconvolution of Thermal and Non-thermal Processes on pCO<sub>2</sub>

The variability of surface pCO<sub>2</sub> caused by thermal and non-thermal processes was estimated from Takahashi et al. (1993, 2002). The method is based on the well-constrained temperature dependence of pCO<sub>2</sub> (4.23%°C<sup>-1</sup>) (Takahashi et al., 1993). It helps to construct the thermally forced seasonal pCO<sub>2</sub> cycle (pCO<sub>2</sub><sup>therm</sup>, Eq. 3) and remove the thermal effect from observed pCO<sub>2</sub> (pCO<sub>2</sub><sup>non-therm</sup>, Eq. 4). We then were able to quantified

the respective influence of  $\delta pCO_2^{therm}$  (pCO<sub>2</sub>–pCO<sub>2</sub><sup>non-therm</sup>) and  $\delta pCO_2^{non-therm}$  (pCO<sub>2</sub>–pCO<sub>2</sub><sup>therm</sup>) on the pCO<sub>2</sub>.

$$pCO_2^{therm} = pCO_{2,mean} \times e^{0.0423 \times (T_{obs} - T_{mean})} \quad (3)$$

$$pCO_2^{non-therm} = pCO_{2,obs} \times e^{0.0423 \times (T_{mean} - T_{obs})} \quad (4)$$

For HF data from the buoy, pCO<sub>2,obs</sub> and T<sub>obs</sub> are the calibrated pCO<sub>2</sub> data (Figure 2 and Supplementary Figure S2) from the SAMI-CO<sub>2</sub> and the SST measured at ASTAN, respectively. pCO<sub>2,mean</sub> is the mean sea surface pCO<sub>2</sub> (420 ± 50 μatm,  $n = 30788$ ) and T<sub>mean</sub> the annual average temperature (13.20 ± 2.09°C,  $n = 33442$ ), calculated from the most complete HF dataset recorded in 2016 and 2019 (Supplementary Table T1). For bimonthly data, means were calculated from January 2015 to December 2019 based on the bimonthly dataset: pCO<sub>2,obs</sub> is the pCO<sub>2</sub> computed from TA/DIC and pH/DIC, with an annual mean of pCO<sub>2,mean</sub> = 410 ± 64 μatm ( $n = 109$ ) at SOMLIT-pier and pCO<sub>2,mean</sub> = 436 ± 39 μatm ( $n = 119$ ) at SOMLIT-offshore. The average temperature observed at SOMLIT-pier was T<sub>mean</sub> = 13.17 ± 2.27°C ( $n = 119$ ) and at SOMLIT-offshore was T<sub>mean</sub> = 13.05 ± 2.04°C ( $n = 121$ ) (Supplementary Table T1).

## Air-Sea CO<sub>2</sub> Fluxes

Atmospheric pCO<sub>2</sub> (pCO<sub>2</sub><sup>air</sup>) was calculated from the CO<sub>2</sub> molar fraction (xCO<sub>2</sub>) from the Mace Head site (53°33' N 9°00' W, southern Ireland) (Figure 1) of the RAMCES network (Observatory Network for Greenhouse gases) and from the water vapor pressure (pH<sub>2</sub>O) using the Weiss and Price (1980) equation. Atmospheric pressure (P<sub>atm</sub>) was obtained from the weather station of the Roscoff Marine Station, and the wind data from the Guipavas meteorological station (48°26'36'' N, 4°24'42'' W, Météo France) (Figure 1). All data were recorded at hourly frequency and then allocated to the HF pCO<sub>2</sub> signal of the ASTAN buoy obtained every 30 min by linear interpolation, daily means were then assigned to discrete values of SOMLIT stations. FCO<sub>2</sub> (in mmol C m<sup>-2</sup> d<sup>-1</sup>, Eq. 5) at the air-sea interface was determined from the difference of pCO<sub>2</sub> between the surface seawater and the air ( $\delta pCO_2 = pCO_2 - pCO_2^{air}$ ), SST, SSS and wind speed.

$$FCO_2 = k \times \alpha \times \delta pCO_2 \quad (5)$$

Where  $k$  represents the gas transfer velocity (m s<sup>-1</sup>) and  $\alpha$  represents the solubility coefficient of CO<sub>2</sub> (mol atm<sup>-1</sup> m<sup>-3</sup>) calculated as in Weiss (1970). The exchange coefficient  $k$  (Eq. 6) was calculated according to the wind speed with the updated algorithm of Wanninkhof (2014) appropriate for regional to global flux estimates and high spatial and temporal resolution of wind products:

$$k = 0.251 \times u_{10}^2 \times \left(\frac{Sc}{660}\right)^{-0.5} \quad (6)$$

Where  $u_{10}$  represents the wind speed at 10 m height (m s<sup>-1</sup>) and  $Sc$  the Schmidt number at *in situ* surface temperature, which varied from 770 to 1250.

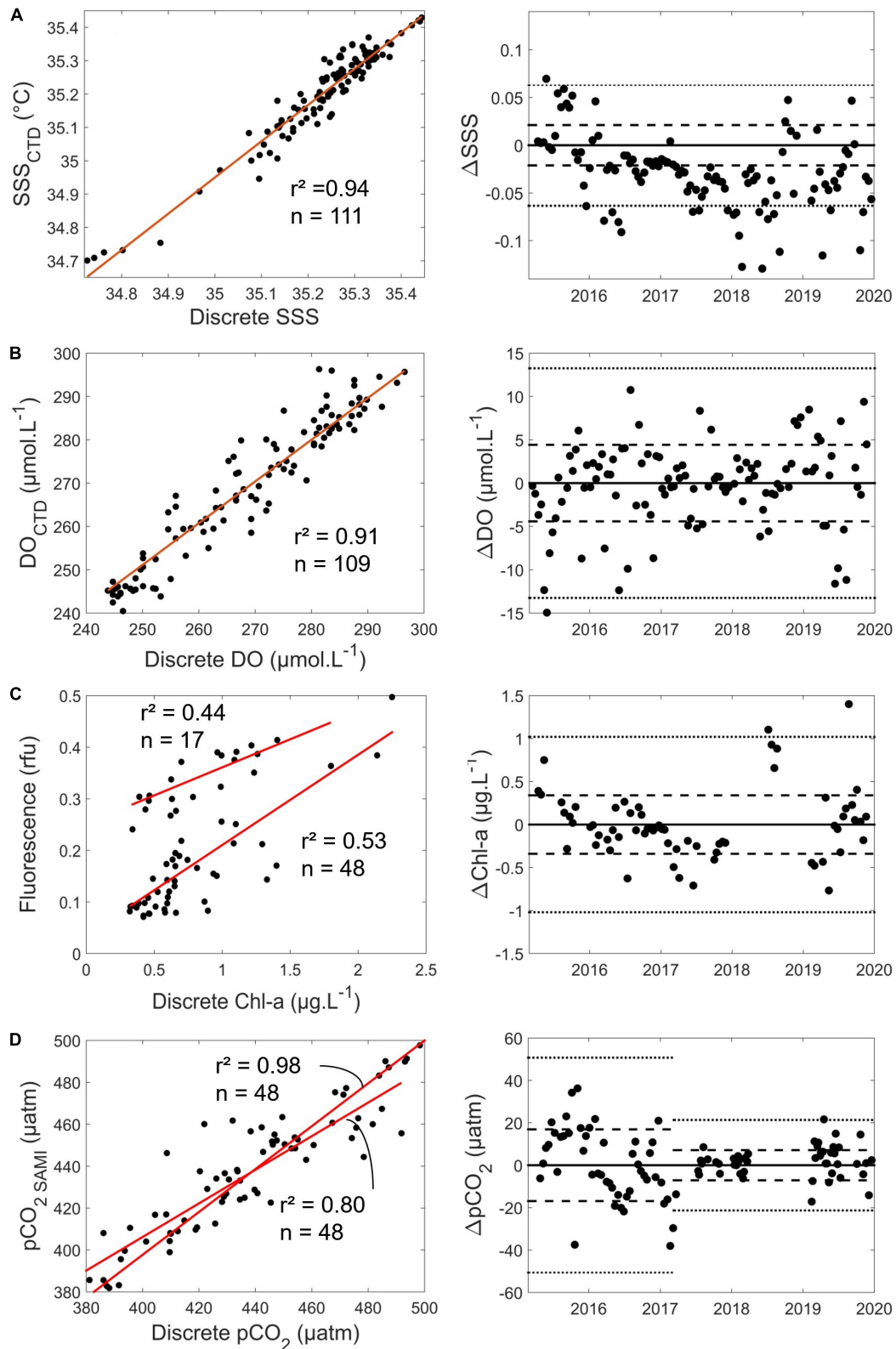


**FIGURE 2 |** Correlations between HF and discrete data for **(A)** SSS, **(B)** DO (μM), **(C)** Chl-a (μg L<sup>-1</sup>), and **(D)** pCO<sub>2</sub> (μatm). Left plots show discrete measurements versus sensor values, with  $n$  the number of discrete measurements, red lines the linear regression between discrete and sensor measurements and associated  $r^2$  values. The right plot shows the differences between sensor values and discrete measurements over time. Dashed lines represent standard deviation of the difference between sensor values and discrete measurements, and dotted lines represent three times the standard deviation.



## Wavelet Analysis

To extract further information on our HF data, mathematical transformations were applied. In 2016 and 2019 the HF dataset covered a major part of the year, and all the studied parameters were measured simultaneously. Wavelet analyses were thus performed on SST, SSS, DO%, and pCO<sub>2</sub><sup>non-therm</sup> to identify the principal frequencies driving the variability of these parameters. Typically, Fourier transforms are used to quantify the constant periodic component in time series. This method is limited when the frequency content changes with time, as in the case of ecological time-series. To overcome these limitations, the wavelets analysis became the norm in environmental time-series analysis, and were used for example to analyze El Nino Southern oscillation (Goring and Bell, 1999) or to follow precipitations distributions (Santos and de Moraes, 2013). Wavelet analysis maintain time and frequency localization in a signal analysis, decomposing a time-series into a time-frequency image. This image, generated as a power spectrum, provides simultaneous information on the amplitude of any periodic signals within the series, and on how this amplitude varies with time (Santos and de Moraes, 2013). Our measurements were carried out at stations influenced by many factors, stationary or not (e.g., tidal range, currents, day–night cycle, marked seasons. . .). In the case of such HF analysis of an environmental signal the continuous wavelet transform (CWT) must be used and the Morlet wavelets are privileged to follow localized scales (Cazelles et al., 2008). The wavelets analysis is also suitable for the analysis of the relationship between two signals, and thus determining the links between each of the environmental variables studied. We used the cross-wavelets transforms to estimate the covariance between each pair of time-series as a function of frequency. The wavelet analyses were carried out from the Matlab package “wavelet-coherence” (Grinsted et al., 2004) on Matlab v2015b.

## RESULTS

### Reliability of the Dataset

From the 06/03/2015 to the 31/12/2019, SST from the Seabird SBE16 + of the ASTAN buoy and from SBE19 + used during discrete sampling at SOMLIT-offshore were very well-correlated ( $r^2 = 0.99$ ,  $n = 99$ , standard deviation of the residuals  $< 0.1^\circ\text{C}$ ) (Supplementary Figure S3). We used the bimonthly discrete measurements of SSS, DO and Chl-a from the SOMLIT-offshore station to determine whether post-calibration of the corresponding sensors of the SBE16 + deployed at the ASTAN buoy was necessary. These samples were collected during high tide slack when the ASTAN and SOMLIT-offshore surface waters had similar biogeochemical properties according to our transect data. The SSS values were in good agreement with discrete salinity measurements with a 1:1 relationship ( $r^2 = 0.95$ ,  $n = 111$ ; standard deviation of the residuals  $< 0.02$ ) (Figure 2A). Similarly, for DO the linear relationship between both measurements was close to 1:1 ( $\text{DO} = 1.03 \cdot \text{DO}_{\text{SBE43}} - 6.7$ ,  $r^2 = 0.91$ ,  $n = 109$ , standard deviation of the residuals  $< 4.4 \mu\text{M}$ ) (Figure 2B). During the 5 years of study, the mean difference between discrete DO and DO measured by the SBE43 sensor was  $0.31 \mu\text{M}$ . In light of these

results, no corrections were applied to the HF SSS and DO. For Chl *a* two different fluorimeters were used during the study, from March 2015 to June 2018 and from June 2018 to December 2019. During the first and second deployments, fluorescence (in relative fluorescence units, RFU) showed significant correlations with discrete Chl-*a* concentrations of (1) Fluorescence =  $0.18 \cdot \text{Chl-}a + 0.04$ ,  $r^2 = 0.52$ ,  $n = 48$  and (2) Fluorescence =  $0.11 \cdot \text{Chl-}a + 0.25$ ,  $r^2 = 0.43$ ,  $n = 17$ , respectively (Figure 2C). Once the two different conversions between fluorescence and Chl-*a* measurements were performed, the standard deviation on the residuals was  $0.34 \mu\text{g L}^{-1}$ . Conversion of *in situ* fluorescence into Chl-*a* concentrations has always been challenging, with fluorescence influenced by numerous factors: heterogeneity of the phytoplankton community structure across the year (Southward et al., 2005; Guilloux et al., 2013), phytoplankton taxonomy (Proctor and Roesler, 2010), cell size (Alpine and Cloern, 1985), pigment packing (Bricaud et al., 1983, 1995; Sosik et al., 1989; Sosik and Mitchell, 1991) and the effect of non-photochemical quenching (Xing et al., 2012). Despite these limitations, Chl-*a* concentrations remains a suitable proxy for phytoplankton biomass (Carberry et al., 2019). The standard deviations obtained on the residuals were close to those obtained with similar sensors on the Armorique Ferry Box between Roscoff and Plymouth (Marrec et al., 2014), therefore no further corrections were applied to the converted Chl *a* signal.

Maintenance of the SAMI-pCO<sub>2</sub> sensor was conducted at least every 3 months and more often during the productive period. Offsets between discrete pCO<sub>2</sub> estimates and SAMI-pCO<sub>2</sub> were detected each time. The offset remained stable during the deployment periods. For example, from the 13/07/2017 to the 31/08/2017, the mean difference between discrete measurements and the sensor was  $+ 8.9 \mu\text{atm}$ , while from 02/10/2017 to 11/01/2018 it was  $-9.9 \mu\text{atm}$ . The pCO<sub>2</sub> values obtained from the sensor were corrected using measured offsets. From March 2015 to March 2017, we used the TA/DIC measurements at SOMLIT-offshore during high tide slack to compute pCO<sub>2</sub>. The pCO<sub>2</sub> values obtained from the sensor were corrected from the measured offset, taking into account the average difference between SOMLIT-offshore and ASTAN buoy. Once the offset was corrected (Figure 2D), we obtained a 1:1 relationship between *in situ* pCO<sub>2</sub> computed from DIC/TA and pCO<sub>2</sub> values given by the SAMI-CO<sub>2</sub> ( $r^2 = 0.80$ ,  $n = 48$ ) with a standard deviation of the residuals of  $16.9 \mu\text{atm}$ . From March 2017 to December 2019, to reduce errors linked to short time and space scales variability, discrete samples for the determination of pH and TA were taken very close to or directly from the buoy at the same depth than the SAMI sensor. We used this pH/TA combination to compute sea surface pCO<sub>2</sub> at the buoy since they provide accurate pCO<sub>2</sub> values (Millero, 2007). We obtained a better 1:1 relationship between *in situ* pCO<sub>2</sub> computed from pH and TA and pCO<sub>2</sub> values given by the SAMI-CO<sub>2</sub> ( $r^2 = 0.98$ ,  $n = 48$ ) with a standard deviation of the residuals of  $7.1 \mu\text{atm}$ .

The percentage of environmental parameters acquired by each sensor had a mean success rate of 60% (Table 1). The SST and SSS mean ratios were most reliable due to the robustness of these sensors. SSTs measured concomitantly by the CTD and the SAMI-CO<sub>2</sub>, were well-correlated (Supplementary Figure S3B).



**TABLE 1** | Percentage of data acquired for each parameter measured at the ASTAN buoy from March 2015 to December 2019.

	SST	SSS	DO	Fluorescence	pCO <sub>2</sub>
2015	67.7%	50.3%	37.8%	47.11%	47.2%
2016	91.0%	88.5%	88.7%	85.9%	60.8%
2017	74.0%	88.8%	57.3%	60.4%	13.2%
2018	75.0%	75.0%	60.1%	0%	25.4%
2019	68.2%	65.9%	35.7%	68.8%	74.5%

DO and fluorescence sensors were more sensitive to specific problems (e.g., biofouling) due to the substantial sensitivity of detection technologies used by these sensors, which are based on polarography (SBE43) and optics (Cyclops C7), respectively. The SAMI-CO<sub>2</sub> was the most impacted sensor in terms of acquisition, principally due to frequent battery shortage, missing reagents, or problems with embedded electronics. With the installation of radio transmission during summer 2018, it was easier to detect breakdowns and therefore quickly undertake repairs. The percentage of data acquisition thus increased for all sensors from this point onwards.

## Physical and Biogeochemical Variability of Coastal sWEC Waters

### Variability of Physical Parameters

Sea surface temperature and SSS showed marked seasonality with cold and fresh water during winter and early spring, and warmer and more saline waters during summer and early fall (**Figures 3A,B**). SST ranged from 9.0°C during winter to 17.0°C during summer. Averaged seasonal SST at SOMLIT-pier was warmer than at SOMLIT-offshore during summer ( $15.89 \pm 0.70^\circ\text{C}$ ,  $n = 31$  vs.  $15.34 \pm 0.66^\circ\text{C}$ ,  $n = 31$ ,  $p$ -value < 0.001), and colder during winter ( $10.44 \pm 0.78^\circ\text{C}$ ,  $n = 36$  vs.  $10.75 \pm 0.76^\circ\text{C}$ ,  $n = 37$ ,  $p$ -value < 0.001) (**Supplementary Table T1**). The seasonal mean of SSS varied from  $\sim 35.15 \pm 0.13$  in winter to  $\sim 35.27 \pm 0.13$  in summer. SSS at SOMLIT-pier was significantly lower than at SOMLIT-offshore because of larger freshwater inputs during the winter with a mean difference of 0.30 (**Supplementary Table T1**). During summer SSS at both stations was in a similar range. At the ASTAN buoy, high-frequency SSS measurements indicated a variability of up to 0.70 within 24 h cycles in winter and up to 0.30 during summer. Interannually, the climatology was calculated from HF daily means of SST and SSS values over 5 years and SST followed a similar pattern between years, except in winter 2018 when the coldest SST was observed, with a 1.5°C difference compared to the 5-year average. SSS did not follow regular seasonality: in 2015 and 2017 SSS followed the 5-year average, with SSS values remaining above 35.0; while in 2016 and 2018, winter SSS decreased down to 34.80 and 34.50, respectively (**Figure 3B**).

### Variability of Chl-a Concentrations and DO%

The SOMLIT-pier DO% and Chl-a were higher than SOMLIT-offshore values, with a mean difference around 2% and 0.05  $\mu\text{g L}^{-1}$  in winter, and around 10% and 0.1  $\mu\text{g L}^{-1}$  in summer. At ASTAN, the variations of HF DO% and converted

Chl-a showed similar dynamics with high DO% > 110%, high Chl-a concentrations (> 2  $\mu\text{g L}^{-1}$ ) during spring, and low Chl-a (< 0.5  $\mu\text{g L}^{-1}$ ) concentrations associated with low DO values close to the equilibrium and/or undersaturated during fall/winter with a mean DO% of  $98.2 \pm 1.6\%$  during winter and values below 93% in November (**Figures 3C,D** and **Supplementary Table T1**). The DO oversaturation generally lasted around 6 months, from April to September, and surface waters were close to equilibrium and/or undersaturated in DO for the rest of the year. High-frequency DO% data recorded at the ASTAN buoy were closer to the data observed at SOMLIT-offshore than at SOMLIT-pier. Both DO% and Chl-a were characterized by high variability when observed from HF measurements, particularly during spring and summer. DO% and Chl-a followed the same general pattern each year but differed temporally. For example DO oversaturation (DO% above 115%) and high Chl-a (5  $\mu\text{g L}^{-1}$ ) were observed in early spring (March) during 2015, but only during late spring (May) in 2018 (**Figures 3C,D**), when large riverine inputs marked by lower SSS values occurred.

### Variability of pCO<sub>2</sub> and FCO<sub>2</sub>

At SOMLIT-offshore and SOMLIT-pier, pCO<sub>2</sub> ranged from 295 to 507  $\mu\text{atm}$  on an annual scale (**Figure 3E**). Minimum values (< 350  $\mu\text{atm}$ ) were observed during spring and early summer, with pCO<sub>2</sub> values below atmospheric equilibrium (pCO<sub>2</sub><sup>air</sup> ranging from 400 to 410  $\mu\text{atm}$ ). Maximum values (> 450  $\mu\text{atm}$ ), above atmospheric equilibrium, were observed during fall and early winter (**Figure 3E**). Surface water CO<sub>2</sub> undersaturation relative to pCO<sub>2</sub><sup>air</sup> lasted around 6 months, from April to September, while CO<sub>2</sub> oversaturation dominated the rest of the year, inversely related to DO%. During summer, pCO<sub>2</sub> at SOMLIT-offshore was higher than at the SOMLIT-pier (+ 65  $\mu\text{atm}$  mean difference), while during winter we observed an opposite pattern (−23  $\mu\text{atm}$  mean difference). HF pCO<sub>2</sub> was generally well-correlated to the low frequency data. However, during May 2016 and 2019 HF data indicated important drawdowns below 300  $\mu\text{atm}$  (related to high Chl *a* values), which were not detected by the low frequency monitoring.

The annual amplitude of FCO<sub>2</sub> (**Figure 3F**) varied from −14 mmol C m<sup>−2</sup> d<sup>−1</sup> to +26 mmol C m<sup>−2</sup> d<sup>−1</sup>. During winter, the fluxes were positive, with surface waters releasing CO<sub>2</sub> to the atmosphere, while the spring negative values revealed a strong absorption of atmospheric CO<sub>2</sub>. During spring, atmospheric CO<sub>2</sub> absorption at the SOMLIT-pier was larger ( $-2.10 \pm 1.80$  mmol C m<sup>−2</sup> d<sup>−1</sup>,  $n = 29$ ) than at SOMLIT-offshore ( $0.29 \pm 1.00$  mmol C m<sup>−2</sup> d<sup>−1</sup>,  $n = 31$ ), with an average difference of 1.8 mmol C m<sup>−2</sup> d<sup>−1</sup> (**Supplementary Table T1**). During winter, the two stations acted rather similarly, with important CO<sub>2</sub> emissions to the atmosphere during the high wind speed periods (e.g., December 2015 and January 2018) (**Figure 3F**). The HF monitoring enabled the observation of important daily FCO<sub>2</sub> variations during the spring of 2015 and 2016. For example, during 2015 HF data revealed values down to −14 mmol C m<sup>−2</sup> d<sup>−1</sup>, compared to the FCO<sub>2</sub> computed from discrete sampling around −4 mmol C m<sup>−2</sup> d<sup>−1</sup>. Similar observations were made during winter 2015, 2016, 2017 and 2019 with, as in 2017, high HF FCO<sub>2</sub> values of 26 mmol C m<sup>−2</sup> d<sup>−1</sup> compared to values of 3 mmol C m<sup>−2</sup> d<sup>−1</sup> computed

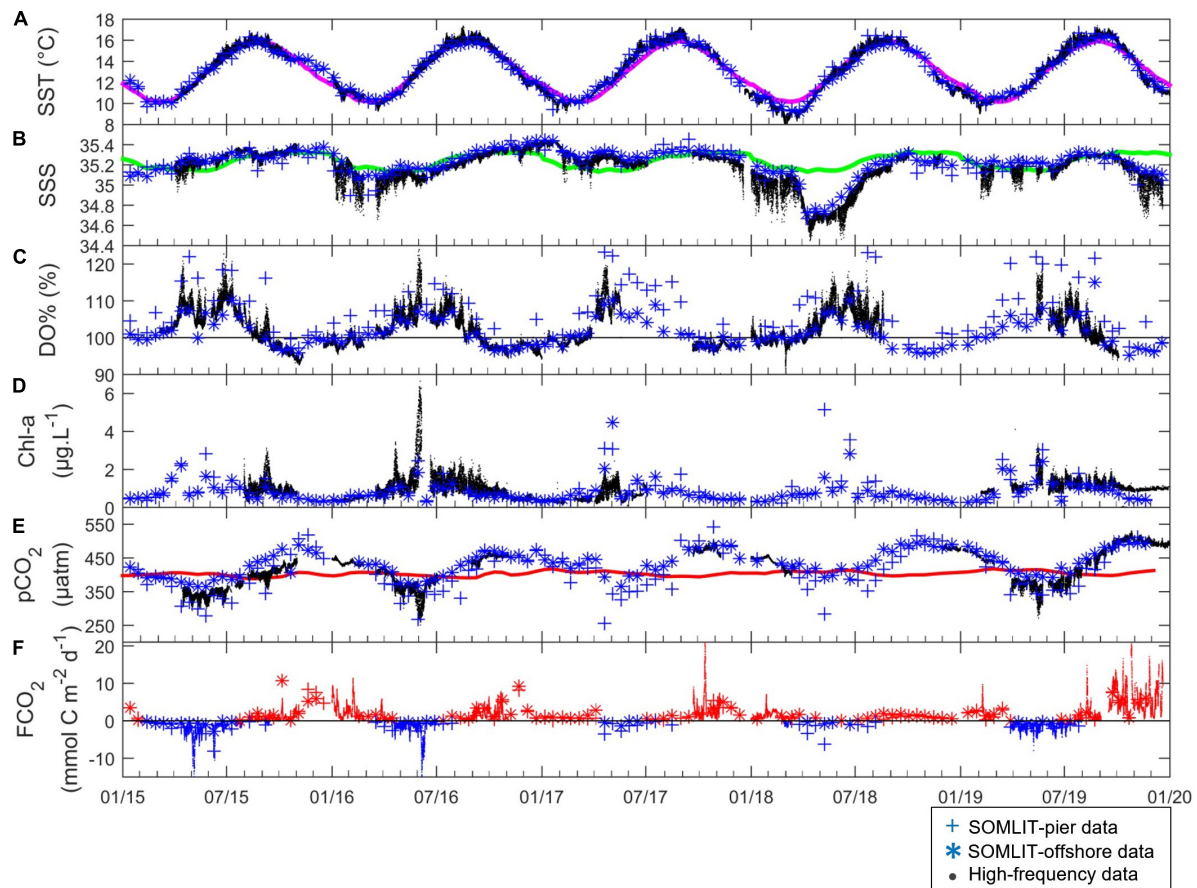


**FIGURE 3** | (• in black) High-frequency, (+ in blue) SOMLIT-pier, and (\* in blue) SOMLIT-offshore data of **(A)** SST (°C), **(B)** SSS, **(C)** DO% (%), **(D)** Chl-a (µg L<sup>-1</sup>), **(E)** pCO<sub>2</sub> (µatm) and **(F)** FCO<sub>2</sub> (mmol C m<sup>-2</sup> d<sup>-1</sup>) from January 2015 to January 2020. Colored lines represent the climatology of **(A)** SST, **(B)** SSS, and the pCO<sub>2</sub><sup>atm</sup> (µatm) on **(E)**. The black lines of **(C,F)** represent the atmospheric equilibrium of DO and CO<sub>2</sub>, respectively. Negative FCO<sub>2</sub> (sink of atmospheric CO<sub>2</sub>) values are represented in blue, and positive FCO<sub>2</sub> (source of CO<sub>2</sub> to the atmosphere) are in red.

from discrete sampling at the same time. Mean seasonal FCO<sub>2</sub> were relatively similar at the three stations during winter, with values between + 2.0 and +4.0 mmol C d<sup>-2</sup> m<sup>-1</sup> (**Figure 4**). The spatial difference was more marked during spring, when FCO<sub>2</sub> was negative at SOMLIT-pier (less than -2 mmol C m<sup>-2</sup> d<sup>-1</sup>) and at ASTAN buoy (around -1.6 mmol C m<sup>-2</sup> d<sup>-1</sup>), but close to equilibrium at SOMLIT-offshore (around -0.3 mmol C m<sup>-2</sup> d<sup>-1</sup>). During summer, SOMLIT-pier and ASTAN buoy had values close to atmospheric equilibrium, while SOMLIT-offshore surface waters released CO<sub>2</sub> at + 1.0 mmol C m<sup>-2</sup> d<sup>-1</sup>. During fall, all sites exhibited large emissions of CO<sub>2</sub> to the atmosphere with values between + 2 and + 6 mmol C m<sup>-2</sup> d<sup>-1</sup>.

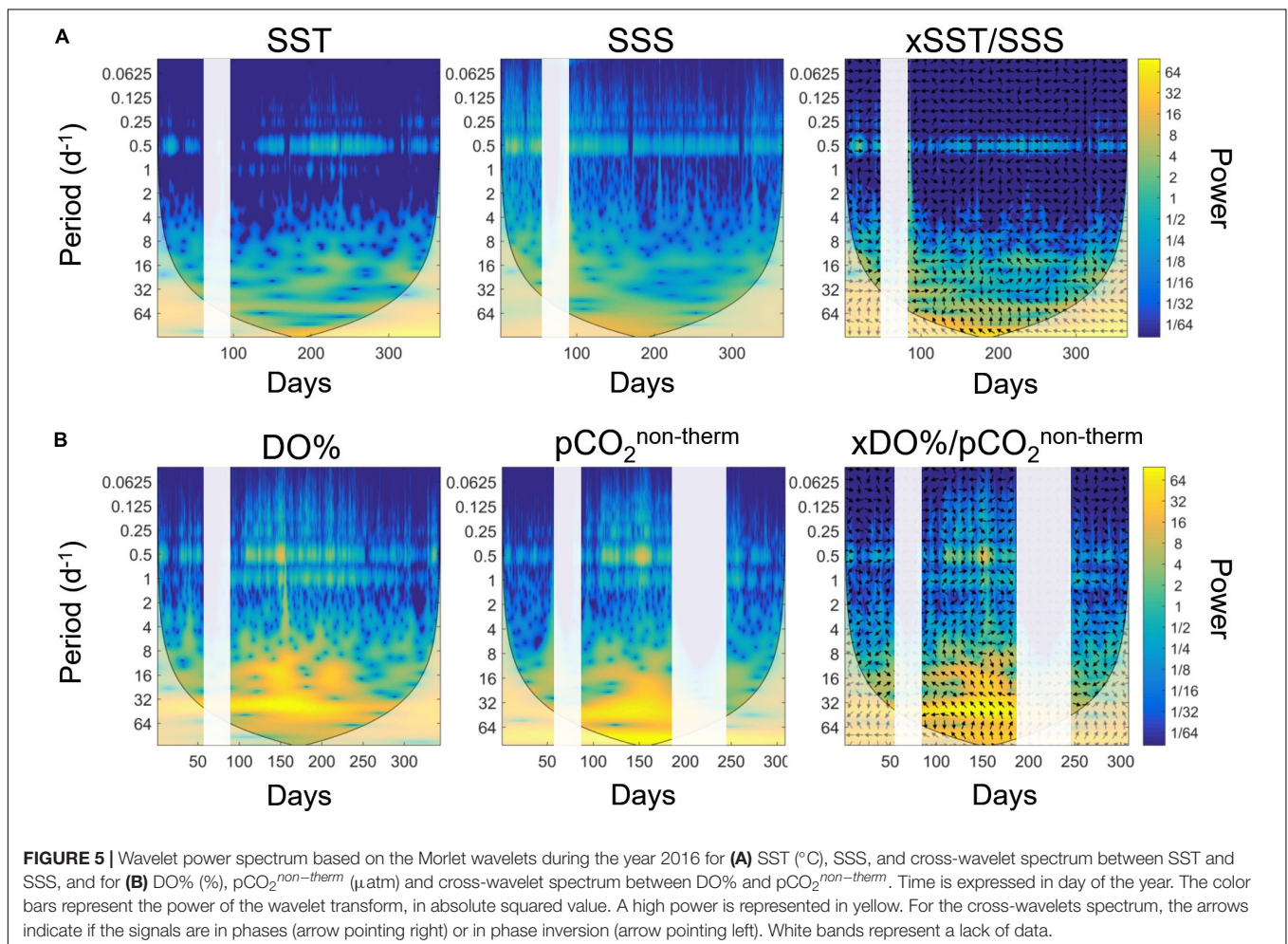
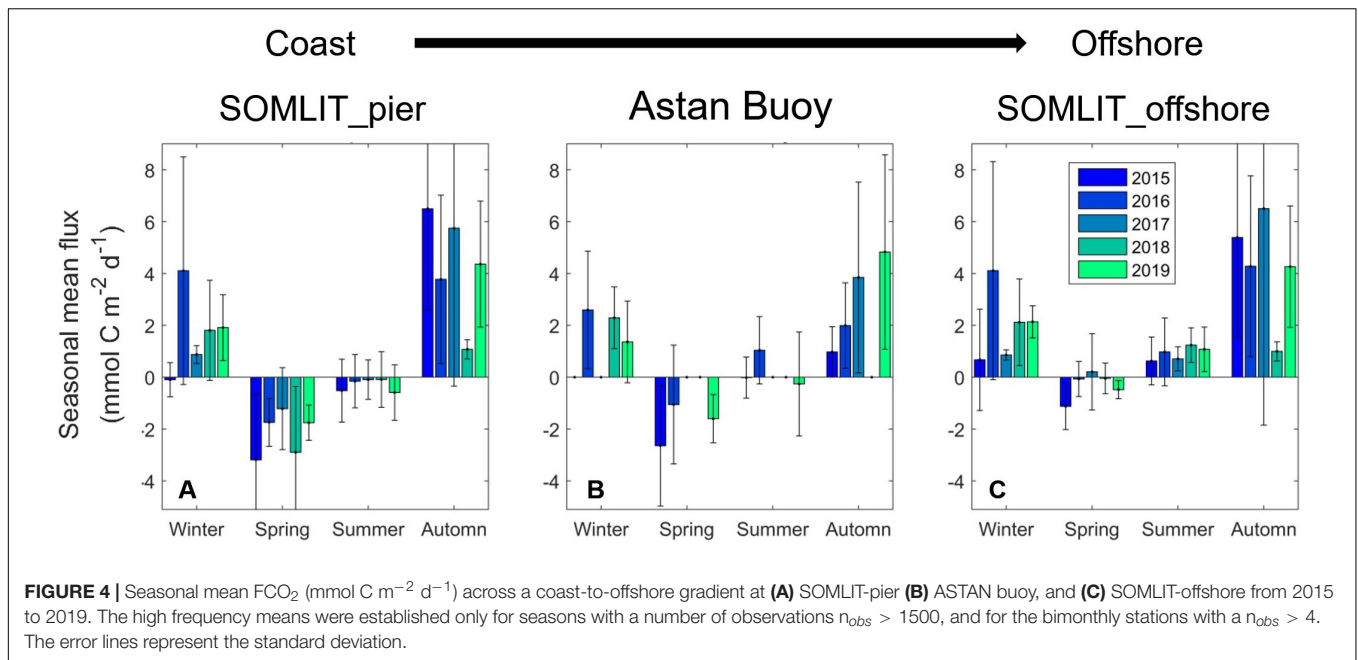
## Frequency Analysis

### Frequency Study of the Physical Structure

Wavelet analyses were applied to the 2016 and 2019 HF SST and SSS data (**Figure 5A**) to identify the main frequencies of variability at the ASTAN buoy. The years 2016 and 2019 were used because the datasets were the most complete. For both years, the SST followed closely the climatology, while the SSS signal was

more variable each year because of the high riverine variability but did not show extreme values as those recorded in 2018.

A 12 h cycle, representative of the tidal period of 0.5 day, clearly appeared on both wavelet analyses throughout the year: high variance values between the signal and the wavelets appeared, indicating more marked correlations during the summer period for SST and during winter for SSS. The diurnal cycle (period of 1 day) appeared weakly and episodically in the wavelet transformation of SST data. The crossed wavelets of SST and SSS highlighted the main periodicity of 0.5 days. At the 12 h frequency, we clearly observed a phase alternation, represented by the change of direction of the arrow, with a signal in phase from October to April, and shifted the rest of the year. The statistical analysis revealed very sharp phase changes and allowed precise pinpointing of the different physical characteristics of two water masses influencing HF measurements. For example, the first inversion started on April 10 during 2016, while the second inversion occurred on November 9 in 2016. Similar analysis for 2019 revealed an inversion on November 7 in 2019, remarkably close in terms of inter-annual variability. These results underline the potential of HF monitoring combined to wavelet analyses





for following shifts in terms of physical regimes in complex nearshore ecosystems.

### Frequency Study of Biogeochemical Parameters

Wavelet transformation for the biogeochemical parameters DO% and pCO<sub>2</sub><sup>non-therm</sup> (Figure 5B), representative of biological processes, revealed two characteristic frequencies of 0.5 and 1 days. These frequencies were more marked during summer compared to winter, with higher power. The cross-wavelet analysis revealed that these two frequencies were identical for both parameters underlying potential diel biological cycles in surface waters at the ASTAN buoy. However, the phases did not show any relevant pattern, and the cross wavelet between the biological and the physical parameters didn't bring more information (not shown). For the 12 h signal, we did not observe distinct regimes similar to those of SST and SSS. In winter, they seemed shifted, with DO% maximal when pCO<sub>2</sub><sup>non-therm</sup> decreased.

### Short-Term Variability of Physical and Biogeochemical Parameters

Short-term variability of HF data recorded at the ASTAN buoy during two representatives 6-days periods in January 2016 and May 2016 is shown in Figure 6. From 05/01/2016 to 10/01/2016 (winter period, Figure 6A), SST ranged from 11 to 14°C, and SSS from 34.85 to 34.95. The SST and SSS varied following 12-h cycles: SST and SSS differences within a 6-h time frame ranged from 0.10 to 0.30°C for SST and from 0.03 to 0.40 for SSS. These two parameters followed the same pattern as the tidal ranges. During high tides SST and SSS reached their highest values, while during low tides minimum SST and SSS values were observed. Similarly, 6-h variation was observed for DO and pCO<sub>2</sub> (Figure 6C). DO ranged from 264 to 274 μM, and pCO<sub>2</sub> ranged from 443 to 457 μatm with a 6-h difference of around 7 μM and 13 μatm, respectively.

From 20/05/2016 to 25/05/2016 (spring period, Figure 6B), SST ranged from 15.80 to 17.20°C, and SSS from 35.18 to 35.25. We observed 6-h variations of SST around 0.40°C, and 6-h variations of SSS around 0.50. SSS followed the tidal variations, and SST was in the opposite phase; i.e., the phase shift highlighted by the wavelet analysis had occurred. DO and pCO<sub>2</sub> patterns were linked to the 12 h tidal cycle, as suggested by the wavelet analysis. During the bloom (Figure 6D), DO ranged from 277 to 290 μM, and pCO<sub>2</sub> from 347 to 379 μatm. 6-h variations were 8 μM for DO and 20 μatm for pCO<sub>2</sub>. pCO<sub>2</sub> was correlated with the tidal pattern, while DO was in the opposite phase. These observations highlight the importance of the tidal cycle in daily variations of biogeochemical parameters at the ASTAN buoy.

## DISCUSSION

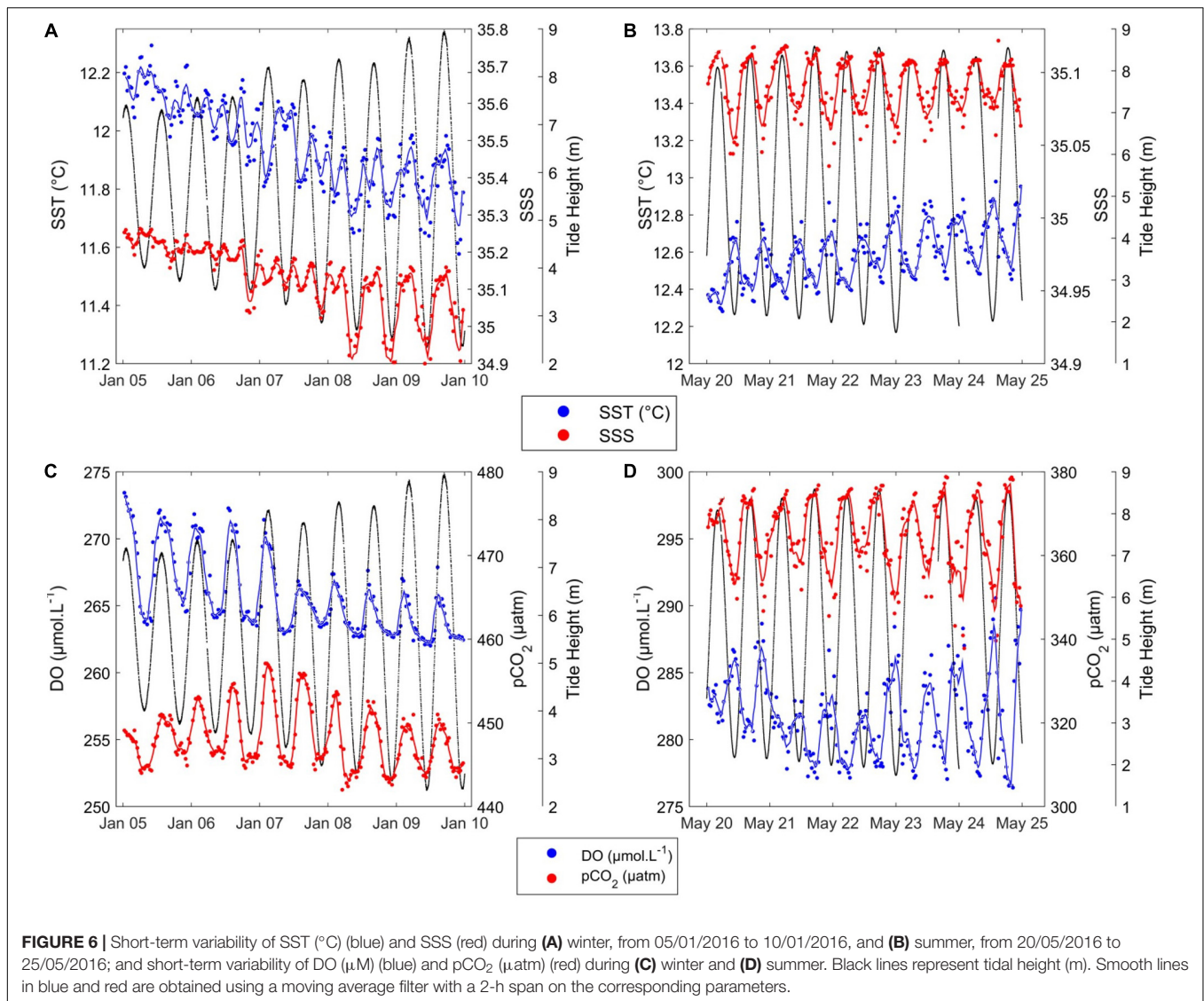
### Short-Scale Variability of the CO<sub>2</sub> System in Coastal sWEC

Discrete data, wavelet analysis and HF data described in Section "Short-Term Variability of Physical and Biogeochemical Parameters" highlighted the tidal transport of two distinct water

masses: firstly a coastal water mass (CWM), unidentified in previous studies (Marrec, 2014), with properties corresponding to the SOMLIT-pier data and present at ASTAN during low tides; secondly an offshore water mass (OWM) corresponding to SOMLIT-offshore data and present at ASTAN during high tides. During the 5 years of observations, the CWM had lower SST during winter, higher SST during summer; and generally lower SSS (Figures 3A,B) (Supplementary Table T1) than the OWM. The phase inversion observed in November and April (Figure 5), which occurred every year, was the consequence of the opposite SST seasonality between the CWM and the OWM (lower SST in summer in OWM and lower SST in winter in CWM). The influence of tides on pCO<sub>2</sub> dynamics is prominent in estuarine ecosystems (De la Paz et al., 2007; Bozec et al., 2012; Oliveira et al., 2018), but has also been observed in various continental shelves of the world ocean (DeGrandpre et al., 1998; Hofmann et al., 2011; Horwitz et al., 2019). Several studies have reported the impact of the tidal cycle on pCO<sub>2</sub> over various European continental shelf provinces, for example in the nWEC (Litt et al., 2010), in the Bay of Brest (Bozec et al., 2011) or in the Cadiz Bay (Ribas-Ribas et al., 2011, 2013). Likewise, enhanced variability at 12-h periods of DO% and pCO<sub>2</sub> were associated to tidal levels and SST/SSS variations at ASTAN (Figures 5, 6). Previous studies were limited to shorter periods of observation, spanning from 20 h to 4 months, with tidal amplitude lesser than 2 m (Litt et al., 2010; Ribas-Ribas et al., 2011, 2013) or to a semi-enclosed bay with limited tidal exchange with the adjacent open ocean (Bozec et al., 2011). During 5 years, we observed mean variations of DO% and pCO<sub>2</sub> around 10% and 15 μatm, respectively, during tidal cycles. The maximum tidal variability associated to spring tides (>7 m) during phytoplankton blooms (16% for DO% and 88 μatm for pCO<sub>2</sub><sup>non-therm</sup>) represented up to 50 and 40% of the respective annual signals at ASTAN. These variabilities reflected the important tidal transport of the CWM and OWM in the coastal sWEC, distinctively revealed by HF monitoring at the ASTAN buoy.

In addition to the tidal variability of DO% and pCO<sub>2</sub> as a result of the presence of distinct water masses at ASTAN, HF monitoring of these biologically dependent variables should also present diurnal variability. During the day, the combination of photosynthesis and respiration is supposed to increase DO% and decrease pCO<sub>2</sub><sup>non-therm</sup>, whereas during the night, respiration processes tend to decrease DO% and increase pCO<sub>2</sub><sup>non-therm</sup>. Borges and Frankignoulle (2003) first revealed a combination of the tidal signal coupled with the biological diel cycle on pCO<sub>2</sub> variations in the English Channel. The impact of the diel cycle on DO%, pCO<sub>2</sub><sup>non-therm</sup> and FCO<sub>2</sub> had also been detected and quantified during the productive period in the nWEC (Marrec et al., 2014). In the adjacent Bay of Brest, HF data showed a maximum of DO% and a minimum of pCO<sub>2</sub> at dusk, and a maximum of pCO<sub>2</sub> and a minimum of DO% at dawn (Bozec et al., 2011). More recently, Liu et al. (2019) highlighted the superimposition of the diel biological signal on the pCO<sub>2</sub> tidal signal in a subtropical tidal estuary. In our case, the main difficulty was to extract the diurnal signal from the high tidal signal, which dominated the short-term variability of pCO<sub>2</sub>, as also observed by Dai et al. (2009) in several





ecosystems of the South China Sea. At the ASTAN site, the diel variability of DO% and pCO<sub>2</sub><sup>non-therm</sup> was indistinguishable due to the prevalence of the tidal signal (**Figure 6**). However, the wavelet analysis revealed a potential day/night cycle for DO% and pCO<sub>2</sub><sup>non-therm</sup> (**Figure 5**), with an important signal on a 24 h period. To estimate the effect of the biological diel cycle on these parameters, we separated the signal, keeping only the data at dusk and dawn according to PAR values measured at the buoy. The day–night differences for DO% and pCO<sub>2</sub><sup>non-therm</sup> clearly appeared during the productive period, when such differences were the most pronounced (**Figure 7**). The data revealed a diel biological cycle with maximum differences of + 5% for DO% and −22 μatm of pCO<sub>2</sub><sup>non-therm</sup> between dawn and dusk. A 10–15 day cycle appeared between day and night variability of DO% and pCO<sub>2</sub><sup>non-therm</sup>, with more pronounced day–night differences at certain periods. This period was closely related to the time when the dawn/dusk cycle was in phase with the low/high tide cycle (data not shown), which means that similar

water masses (CWM or OWM) were in vicinity of the ASTAN buoy at dusk and dawn. The annual mean difference of the day/night DO% was 0.6%, and 3 μatm for pCO<sub>2</sub><sup>non-therm</sup>, remaining rather low compared to tidal variability. However, when considering the maximum wavelet amplitude of %DO and pCO<sub>2</sub><sup>non-therm</sup> during the bloom (Day ~140 corresponding to May, **Figure 5**), the day/night signal accounted for 30% of the annual variation of DO% and for 9% of the annual variation of pCO<sub>2</sub><sup>non-therm</sup>. As well as revealing the significant tidally induced variability of the pCO<sub>2</sub> signal, HF monitoring of coastal sWEC waters provided key information about the impact of the diel biological cycle on the CO<sub>2</sub> system.

Combining HF measurements of pH or pCO<sub>2</sub> with discrete carbonate system parameters (DIC/TA) can be a valuable tool for carbon cycle research based on autonomous mooring (Cullison Gray et al., 2011). Our robust TA/SSS relationship established in Section “Carbonate System Parameters” was concordant with similar relationships estimated in North Atlantic waters mixing

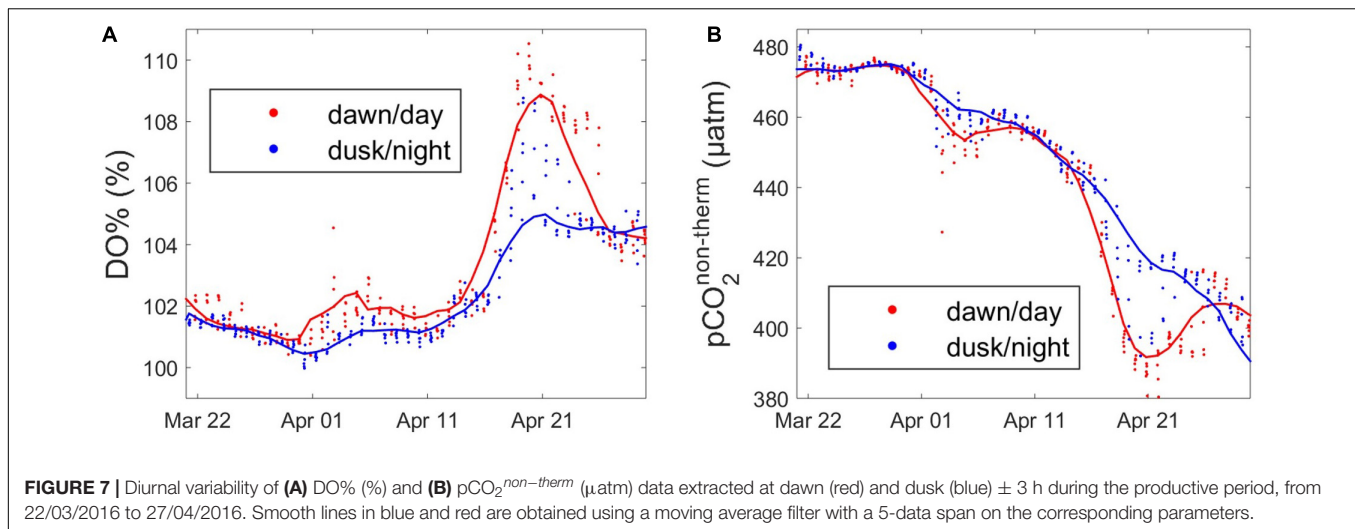


**FIGURE 7 |** Diurnal variability of (A) DO% (%) and (B)  $p\text{CO}_2^{\text{non-therm}}$  ( $\mu\text{atm}$ ) data extracted at dawn (red) and dusk (blue)  $\pm 3$  h during the productive period, from 22/03/2016 to 27/04/2016. Smooth lines in blue and red are obtained using a moving average filter with a 5-data span on the corresponding parameters.

with freshwater from non-limestone Irish rivers with similar TA end members (McGrath et al., 2016). We therefore estimated HF  $\text{pH}_{\text{calc}}$  for 2016, which varied from 8.00 during winter to 8.20 during summer (Figure 8A). These values were within the range of the *in situ* pH estimated between 7.97 and 8.35 by Marrec (2014) in the WEC and with pH values reported by McGrath et al. (2019) in Irish coastal waters (between 8.00 and 8.30). Unsurprisingly,  $\text{pH}_{\text{calc}}$  exhibited opposite dynamics to  $p\text{CO}_2$  and was strongly related to the tidal signal. During spring/summer, low  $\text{pH}_{\text{calc}}$  values were observed at high tide and high  $\text{pH}_{\text{calc}}$  values at low tide, with 12-h variations up to 0.12 units (Figure 8B). The pH variability is particularly intense in coastal ecosystems (Ostle et al., 2016; Brodeur et al., 2019) resulting from various biogeochemical and physical processes (Waldbusser and Salisbury, 2014). In this study, most of the variability of  $\text{pH}_{\text{calc}}$  observed at the ASTAN site during spring likely resulted from tidal transport of the CWM and the OWM with contrasting biological and physical properties.

Hydes et al. (2011) reported long-term pH decrease of  $-0.002$  to  $-0.004$  pH unit  $\text{yr}^{-1}$  from 1995 to 2009 in the northwest European continental shelf, higher than in the Atlantic waters (Kitidis et al., 2017) and in the open ocean (Doney et al., 2009). At a daily time-scale, we observed variations up to 6 times greater than this regional annual acidification trend, and the seasonal variation was 10 times greater than the decadal change in the area. These strong variabilities are similar to the observations of McGrath et al. (2019) who reported, in similar coastal ecosystems in Ireland, a pH variability from 10 to 50 times greater than the decadal change linked to OA. Large changes of  $p\text{CO}_2$  and pH were previously observed during short measurements period at fixed locations in various coastal ecosystems (Hofmann et al., 2011; Saderne et al., 2013). Intense changes in pH and saturation state  $\Omega_{\text{arag}}$  have also been reported at coastal mooring sites in the California Current Ecosystem with natural variability overlapping with preindustrial conditions but also revealing critical OA conditions (Sutton et al., 2016). This variability has direct implications for calcifying species because variable pH exposure can affect organism response to OA (Vargas

et al., 2017). Extremes decrease of  $\Omega_{\text{arag}}$  have also been related to pteropods shell dissolution (Feely et al., 2016) and identified as a potential threat for the shellfish industry (Salisbury et al., 2008). Marine organisms in regions of persistent low pH might be locally adapted to OA (Sanford and Kelly, 2011; Pespeni et al., 2013). However, knowledge gaps about when and where corrosive conditions occur (Feely et al., 2016; Chan et al., 2017; Fennel et al., 2019) and how the timing of such conditions relates to key life stages (Legrand et al., 2017; Kapsenberg et al., 2018) still have to be filled to assess vulnerability to OA. Here we showed large daily changes in pH/ $p\text{CO}_2$  but also DO/SST at the ASTAN mooring associated with the tidal transport of the CWM and the OWM in the nearshore area of the WEC over 5 years. These data can improve experimental design to evaluate organism response under real-world conditions by submitting these organisms to realistic variability in carbonate parameters (Chan et al., 2017) but also to varying DO and SST (Reum et al., 2016) instead of previous classical experimental designs (Noisette et al., 2016; Legrand et al., 2017) used in the WEC.

## Seasonal and Interannual Control of $p\text{CO}_2$ in Coastal sWEC

Previous studies investigating the seasonal patterns of  $p\text{CO}_2$  in the WEC indicated important physical and biological influence on carbonate cycling (Borges and Frankignoulle, 2003; Padin et al., 2007; Dumousseaud et al., 2010; Litt et al., 2010; Kitidis et al., 2012). With our 5 years of HF and discrete data we further investigated the seasonal and inter-annual variability of  $p\text{CO}_2$  in the proximal area of the sWEC. Following the approach proposed by Takahashi et al. (1993, 2002), we discriminated the influence of thermal processes ( $p\text{CO}_2^{\text{therm}}$ ) from non-thermal processes ( $p\text{CO}_2^{\text{non-therm}}$ ) (Figures 9A,B) and we quantified the respective influence of  $\delta p\text{CO}_2^{\text{therm}}$  and  $\delta p\text{CO}_2^{\text{non-therm}}$  on  $p\text{CO}_2$  (Figure 9C).

The SST followed a rather regular pattern every year with limited inter-annual variations. Since  $p\text{CO}_2^{\text{therm}}$  is mainly influenced by temperature, we observed a variation of  $p\text{CO}_2^{\text{therm}}$

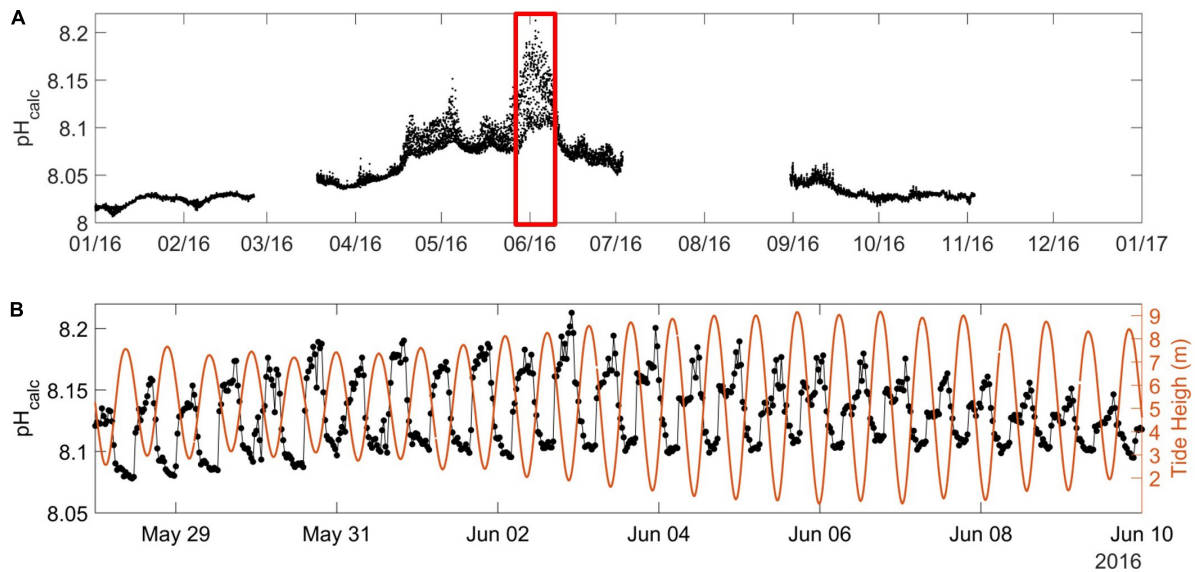


**FIGURE 8 | (A)**  $\text{pH}_{\text{calc}}$  (in pH units on the total scale at *in situ* SST) at the ASTAN buoy during the year 2016 as explained in Section “Carbonate System Parameters” with **(B)** emphasis on the spring short-term variability of  $\text{pH}_{\text{calc}}$  (black dot) and the water level [in meters (orange line)] from 28/05/2016 to 09/06/2016.

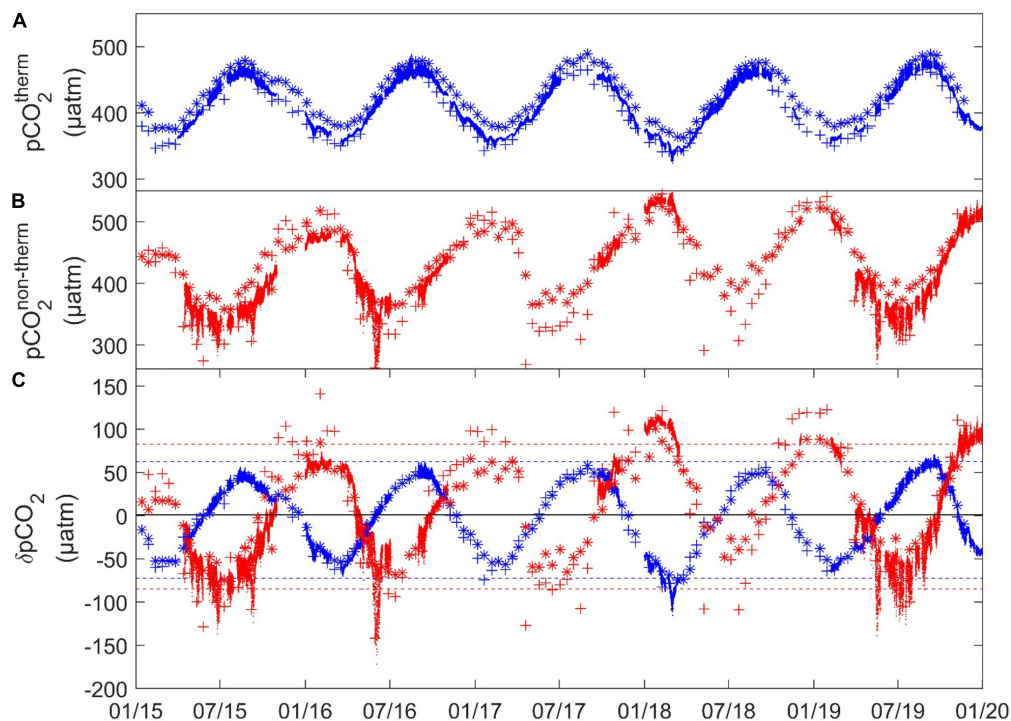


**FIGURE 9 | (A)**  $\text{pCO}_2^{\text{therm}}$  (blue), **(B)**  $\text{pCO}_2^{\text{non-therm}}$  (red) **(C)**  $\delta\text{pCO}_2^{\text{therm}} = \text{pCO}_2 - \text{pCO}_2^{\text{non-therm}}$  (blue) and  $\delta\text{pCO}_2^{\text{non-therm}} = \text{pCO}_2 - \text{pCO}_2^{\text{therm}}$  (red) (all in  $\mu\text{atm}$ ) for (.) High-frequency, (+) SOMLIT-pier, and (\*) SOMLIT-offshore data. Dashed lines represent the maximum and minimum of the monthly mean of  $\delta\text{pCO}_2^{\text{therm}}$  (blue) and  $\delta\text{pCO}_2^{\text{non-therm}}$  (red).

mirroring SST variations, varying from 325 to 490  $\mu\text{atm}$  during winter and summer, respectively.  $\delta\text{pCO}_2^{\text{therm}}$  varied from + 67  $\mu\text{atm}$  due to increasing SST during summer to −104  $\mu\text{atm}$  due to decreasing SST during winter. In 2018, winter

values diverged from the other years with lower SST (−1.5°C) compared to average values. Therefore, the lowest  $\text{pCO}_2^{\text{therm}}$  values (around 345  $\mu\text{atm}$ ) and a  $\delta\text{pCO}_2^{\text{therm}}$  of −104  $\mu\text{atm}$  (20  $\mu\text{atm}$  lower than the other years) were encountered that



year. It is worth noting that during the same period SSS largely diverged from the average with values as low as 34.60, only recorded by HF monitoring. The decrease of pCO<sub>2</sub> induced by thermal processes was counterbalanced by particularly high pCO<sub>2</sub><sup>non-therm</sup> values at this time (>500 μatm). The strong impact of non-thermal processes in winter 2018 might be related to intense riverine inputs, which brought a large amount of organic material. Besides this interannual variability, the 5-year dataset at the two discrete stations revealed spatial variability of the thermal effect on pCO<sub>2</sub>. During winter, pCO<sub>2</sub><sup>therm</sup> was lower at SOMLIT-pier (or CWM) compared to SOMLIT-offshore (or OWM), due to stronger cooling of nearshore waters during the winter regime. δpCO<sub>2</sub><sup>therm</sup> revealed an impact 7 μatm higher of the SST cooling on pCO<sub>2</sub> in the CWM (**Supplementary Table T1**). During summer, after the shift from the winter to the summer regime, SST was higher at SOMLIT-pier than at SOMLIT-offshore. δpCO<sub>2</sub><sup>therm</sup> showed that this higher SST was responsible for a potential increase of 5 μatm of pCO<sub>2</sub> in CWM compared to OWM (**Supplementary Table T1**).

Non-thermal effects on pCO<sub>2</sub>, pCO<sub>2</sub><sup>non-therm</sup>, are strongly influenced by biological production/respiration processes, but also by factors such as lateral advection, vertical mixing, air-sea CO<sub>2</sub> exchanges, dissolution/formation of CaCO<sub>3</sub>, sediment/water-column interactions, or riverine inputs. However, this parameter remains a valuable and efficient approach to assess the impact of biological processes on pCO<sub>2</sub> variability (Thomas et al., 2005). Windspeed data (**Supplementary Figure S4**) showed a rather stable signal (higher values during winter's storms and lower values during spring/summer) throughout the 5 years of study, which did not induce large inter-annual pCO<sub>2</sub><sup>non-therm</sup> variability. The HF data showed a clear opposite dynamic between Chl-a-DO%, and the pCO<sub>2</sub><sup>non-therm</sup> signals both temporally and in terms of intensity. The opposite patterns indicated that pCO<sub>2</sub><sup>non-therm</sup> could reasonably be considered as an indicator to quantify the effect of biological processes on natural pCO<sub>2</sub> variability.

Spring in the sWEC is characterized by phytoplankton blooms between March and April fueled by the winter nutrient stock. The onset of spring phytoplankton blooms depends on light availability throughout the well-mixed water column (Wafar et al., 1983; L'Helguen et al., 1996). Surface waters, and the entire water column (except when weak and short stratification occurred), still exhibited relatively high Chl-a concentrations and oversaturated DO% along the summer since nutrient stocks (particularly nitrate) are rarely totally depleted because of the light limitation induced by strong mixing (Wafar et al., 1983; L'Helguen et al., 1996; Marrec, 2014). In fall, light availability becomes insufficient to support the substantial level of primary production required to maintain DO% oversaturation. Respiration and remineralization processes therefore become the main driver of pCO<sub>2</sub> variability, consuming DO, releasing CO<sub>2</sub>, and driving the nutrient concentrations as in other temperate ecosystems of the northwest European continental shelf (Bozec et al., 2011; Marrec et al., 2013; Salt et al., 2016; Hartman et al., 2019). The biologically productive periods were accompanied by DO% > 100% and Chl-a concentrations > 1 μg L<sup>-1</sup> from April to October every year, with oxygen saturation

reaching values up to 120%. During winter the heterotrophic activity (respiration and remineralization of organic matter) dominated with much lower Chl-a and undersaturated DO%. δpCO<sub>2</sub><sup>non-therm</sup> showed a regular pattern driven by these production/respiration processes, with a strong coupling between the start/end of < 0 δpCO<sub>2</sub><sup>non-therm</sup> and > 100% DO% values, and proved to be a suitable indicator of the extent and duration of the productive period (**Figure 9C**).

Important interannual variability was observed with respect to the onset and end of the productive period, as indicated by the DO% and δpCO<sub>2</sub><sup>non-therm</sup> signals. In 2015, DO% started to be significantly higher than 100% in March, synchronized with an increase of Chl-a, and surface waters remained oversaturated in DO up to mid-September, while in 2018, the productive period started in May and ended in late August. 2018 was characterized by larger freshwater inputs (**Figure 3B**) due to heavy precipitations in late winter/early spring, and thus reduced light availability, associated with greater turbidity, which might have limited light penetration in the mixed water-column and thus delayed the start of the productive period. The pCO<sub>2</sub><sup>non-therm</sup> and δpCO<sub>2</sub><sup>non-therm</sup> signals followed similar dynamics. In 2015, pCO<sub>2</sub><sup>non-therm</sup> and δpCO<sub>2</sub><sup>non-therm</sup> started to decrease and to be negative, respectively, in April, whereas negative δpCO<sub>2</sub><sup>non-therm</sup> started to be observed in May in 2018. Positive δpCO<sub>2</sub><sup>non-therm</sup> values were observed from September in 2015 and from August in 2018. The decrease of pCO<sub>2</sub><sup>non-therm</sup> in spring can be particularly rapid, as in spring 2016 with a drawdown of around 250 μatm during a 2-month period (March–May), revealing a large consumption of pCO<sub>2</sub> by biological activity partly counteracted by the increasing SST and pCO<sub>2</sub><sup>therm</sup> at the same period.

Spatial variability was visible from the discrete data, particularly in summer, when pCO<sub>2</sub><sup>non-therm</sup> was persistently lower at SOMLIT-pier (CWM) than at SOMLIT-offshore (OWM). During the productive period, seasonal minimal δpCO<sub>2</sub><sup>non-therm</sup> values lower than −100 μatm were observed in the CWM every year, while the δpCO<sub>2</sub><sup>non-therm</sup> signals never reached values below −70 μatm in the OWM. The shallower depth in the CMW favors light penetration, which can result in higher pelagic production (when nutrients are not depleted) compared to the deeper OWM. The role of benthic production processes on CO<sub>2</sub> variations is also important in proximal shallow areas (Hammond et al., 1999; Cai et al., 2000; Forja et al., 2004; Waldbusser and Salisbury, 2014; Oliveira et al., 2018). The low δpCO<sub>2</sub><sup>non-therm</sup> associated to CWM during the productive period might include both higher pelagic and benthic production, with a predominance of the latter. The tidal transport of the CWM over adjacent seagrass and macroalgae beds with high CO<sub>2</sub> consumption (Ouisse et al., 2011; Bordeyne et al., 2017) extended the biological productive period of the CWM to the benthic compartment. The δpCO<sub>2</sub><sup>non-therm</sup> seasonal mean difference of 30 μatm recorded between both stations was therefore a gross estimation of the benthic compartment production within the nearshore area. Similarly, a nearshore to offshore gradient was observed during fall and early winter. Values of δpCO<sub>2</sub><sup>non-therm</sup> in the CWM of 130 μatm were 40 μatm higher than in the OWM, the important benthic and pelagic remineralization in the



shallower CWM contributing to a larger increase of pCO<sub>2</sub>. This increase was partly counteracted by the decreasing pCO<sub>2</sub><sup>therm</sup> due to fall and winter SST cooling as discussed above.

Our data revealed a somewhat classical picture of pCO<sub>2</sub> control in temperate ecosystems with counteracting effects of thermodynamic and biological activity depending on the seasons (Thomas et al., 2005; Bozec et al., 2011). The combined 5-year HF and discrete data allowed for the first time the quantification of rather large interannual and spatial variability in the proximal surface waters of the sWEC. Non-thermal processes, that we assumed to be mainly controlled by biological activity, were the main driver of pCO<sub>2</sub> in the coastal sWEC, as shown by the larger amplitude, both during winter and summer, of pCO<sub>2</sub><sup>non-therm</sup> compared to pCO<sub>2</sub><sup>therm</sup>. The interannual variability of pCO<sub>2</sub> depended mainly on the duration and the intensity of the productive period. The weak interannual variability in terms of SST limited its control over the 5 years of study on pCO<sub>2</sub> compared to production/respiration processes.

## Dynamics of FCO<sub>2</sub> in the WEC

Our study provides FCO<sub>2</sub> estimates at daily, seasonal and annual time scales. One major limitation for estimating HF FCO<sub>2</sub> is the requirement to access HF atmospheric CO<sub>2</sub> data in the surrounding study area. Northcott et al. (2019) recently demonstrated the impact of higher atmospheric CO<sub>2</sub> transported by offshore winds from urban and agricultural land on FCO<sub>2</sub> estimates in Monterey Bay, California. This concern was also addressed by Wimart-Rousseau et al. (2020) in their study of FCO<sub>2</sub> in the vicinity of a highly urbanized area. Unfortunately, we did not have access to local HF atmospheric CO<sub>2</sub> data, so atmospheric xCO<sub>2</sub> data from the RAMCES network collected at the Mace Head site (53°33' N 9°00' W, southern Ireland) were used to calculate pCO<sub>2</sub><sup>atm</sup>. The dominant onshore south-westerly winds and rather lowly urbanized surroundings in our study area mean that the Mace Head record should be representative of our study site. The use of local wind products from the nearby Guipavas weather station (**Supplementary Figure S4**) and of recent gas transfer velocity parametrization adapted to regional estimates (Wanninkhof, 2014) limited the error linked to different wind products in regional air-sea flux estimations (Roobaert et al., 2018). The impact of rain, extreme wind events and associated bubble entrainment, surface films or boundary layer stability (Wanninkhof et al., 2009 for a review) are factors inducing additional uncertainty into gas transfer velocity *k*, and therefore HF FCO<sub>2</sub> calculation, but remain particularly difficult to assess. The eddy covariance technique, as used by Yang et al. (2019) in the nWEC, can overcome most of these limitations inherent to gas transfer velocity parametrization, and presents some undeniable advantages for studying HF FCO<sub>2</sub>. However, the use of *in situ* seawater pCO<sub>2</sub> sensor remained the most effective way to study pCO<sub>2</sub>, examine its control, and simultaneously estimate air-sea CO<sub>2</sub> fluxes using widely used wind dependent gas transfer velocity parametrization.

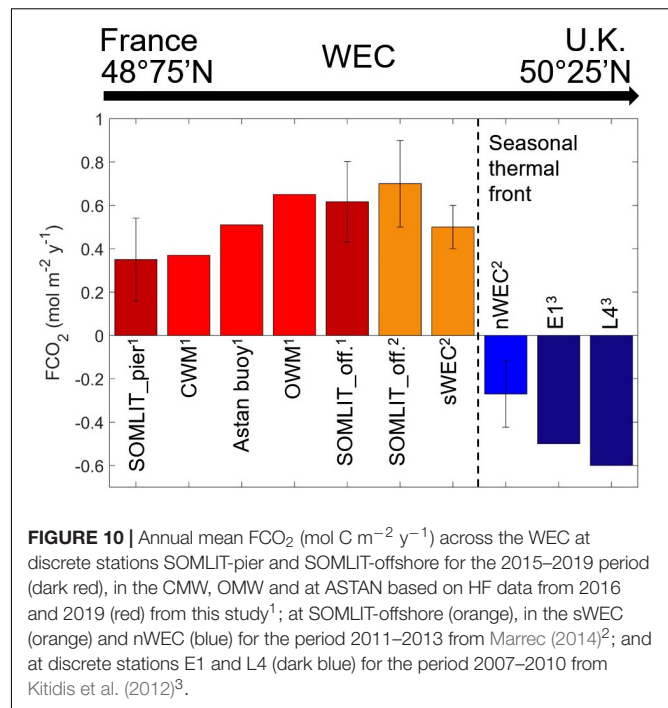
The main benefit of HF data was to assess daily FCO<sub>2</sub> variability and capture extreme events such as high fluxes observed during winter or abrupt shifts and drawdown during spring. For example, during winter 2017 a HF FCO<sub>2</sub> of 26 mmol

C m<sup>-2</sup> d<sup>-1</sup> was recorded at ASTAN compared to values of 3 mmol C m<sup>-2</sup> d<sup>-1</sup> computed from discrete values at the same time. During spring, as explained in Section “Seasonal and Interannual Control of pCO<sub>2</sub> in Coastal WEC,” the large interannual variability of the intensity and trigger of spring blooms was responsible for variable spring drawdown in pCO<sub>2</sub>, revealing sudden and strong inversions of the fluxes. For example, in March 2016 FCO<sub>2</sub> was on average positive with a monthly maximum of + 5.93 mmol C m<sup>-2</sup> d<sup>-1</sup> (03/27/16), and within a few days became negative, with a monthly minimum of -4.42 mmol C m<sup>-2</sup> d<sup>-1</sup> (04/19/16). This large daily variability should be taken into account when considering the spring average carbon sink for each year (with a mean estimate at -2.12 mmol C m<sup>-2</sup> d<sup>-1</sup>). With the method applied in Section “Short-Scale Variability of the CO<sub>2</sub> System in Coastal sWEC” we were able to separate the day/night signal during this period and found a mean difference of FCO<sub>2</sub> of -0.12 mmol m<sup>-2</sup> d<sup>-1</sup> due to the diel biological cycle. This estimation was understandably lower than the day-night difference estimated at -0.90 mmol m<sup>-2</sup> d<sup>-1</sup> for FCO<sub>2</sub> during spring in the stratified and more productive nWEC (Marrec et al., 2014). FCO<sub>2</sub> based on HF data provided relevant information on short-term variability, the main caveat of the cardinal buoy data being the significant loss of data, which hindered computation of mean seasonal averages.

The mean seasonal FCO<sub>2</sub> values for the three sites during the 5 years of study were compared to assess the seasonal and spatial variability of FCO<sub>2</sub> along a coastal/offshore gradient (**Figure 4**). FCO<sub>2</sub> computed from the HF data at ASTAN exhibited similar overall variability as FCO<sub>2</sub> obtained from discrete measurements at SOMLIT-pier (CWM) and at SOMLIT-offshore (OWM). Similar general patterns between HF and discrete data at the seasonal level have also been reported in recent studies (Shadwick et al., 2019). Regardless of sampling frequency and locations, the three studied sites acted as strong sources of CO<sub>2</sub> to the atmosphere during winter/fall. During spring, SOMLIT-pier and ASTAN acted as sinks of atmospheric CO<sub>2</sub>, with higher CO<sub>2</sub> sink at SOMLIT-pier than at ASTAN, while fluxes computed at SOMLIT-offshore indicated exchanges near equilibrium. Summer was the only time of the year when significant differences in terms of flux intensity and direction were observed between the three sites. This time of the year corresponds to the shift from dominant production of organic matter by photosynthetic organisms toward dominant remineralization and respiration processes, which usually start earlier in the deeper well-mixed water column at SOMLIT-offshore. The 2015/2018 years were marked by large differences in terms of the date of onset and length of the productive period, which were poorly reflected in the mean seasonal spring and summer FCO<sub>2</sub>. However, the following fall was marked by large differences in terms of emissions of CO<sub>2</sub> to the atmosphere, much lower in 2018 compared to 2015 when it was driven by high wind speeds (maximum monthly mean of 9.7 m s<sup>-1</sup>). The mean wind speeds recorded during fall 2018 (4.6 m s<sup>-1</sup>) were followed by lower than average wind speeds the following winter months (4.6 m s<sup>-1</sup> compared to mean 5.2 m s<sup>-1</sup>) (**Figure 3**), which still resulted in significant flux differences, driven this time by the

delayed remineralization period (Figure 4). This study confirms that seasonal variability of FCO<sub>2</sub> in this part of the NE European continental shelf is controlled by complex interactions between high/low wind speeds, production/respiration of organic matter and winter cooling (Kitidis et al., 2019).

On an annual basis, given the dominant impact of the tidal cycle at ASTAN, it seemed particularly interesting to assess the proximal coastal/offshore gradient of FCO<sub>2</sub> from the buoy data only. In 2016/2019 the HF dataset was sufficiently complete to attempt an estimation of annual FCO<sub>2</sub> in the CMW and OWM based on tidal separation of the HF signal. We separated the dataset according to high tides (>8 m) and low tides (<2.5 m), as previously explained. The annual mean FCO<sub>2</sub> over 2016/2019 was estimated at 0.37 mol C m<sup>-2</sup> yr<sup>-1</sup> for the CMW and 0.65 mol C m<sup>-2</sup> yr<sup>-1</sup> for the OWM (Figure 10). The mean HF FCO<sub>2</sub> of 0.51 mol C m<sup>-2</sup> yr<sup>-1</sup> for 2016/2019 at the ASTAN buoy was obviously within the range of FCO<sub>2</sub> in the CMW and OWM. FCO<sub>2</sub> computed at ASTAN comprised both the tidal and diurnal signals and was therefore representative of nearshore surface waters in the sWEC. Comparison of these HF budget with the annual mean budget for 2016/2019 based on discrete sampling at SOMLIT-pier (0.35 mol C m<sup>-2</sup> yr<sup>-1</sup>) and SOMLIT-offshore (0.62 mol C m<sup>-2</sup> yr<sup>-1</sup>), which we assumed representative of the CWM and OWM, respectively, revealed very similar values. Here, the arbitrary separation of the HF data according to tide levels provided coherent results with discrete samples collected at noon during neap tides at both SOMLIT stations. We were able to estimate FCO<sub>2</sub> in the CWM and OWM with the ASTAN mooring, which underly the great potential of cardinal buoys to capture the dynamic of FCO<sub>2</sub> in nearshore tidal ecosystems. It is worth noting that CO<sub>2</sub> emissions at SOMLIT-offshore (averaged over the 5-year period) showed a similar trend but lower values than emissions computed from 2011 to 2013 at the same site (Figure 10), with an atmospheric CO<sub>2</sub> increase of +9 to +15 μatm recorded between the studies. These new estimates in nearshore waters of the sWEC over a 5-year period combined with previous studies provided a full latitudinal representation over multiple years for FCO<sub>2</sub> in the WEC (Figures 1, 10). This is particularly relevant since proximal areas are currently excluded from global estimates in the coastal ocean (Bourgeois et al., 2016). The latitudinal comparison showed a clear gradient from a weak source of CO<sub>2</sub> in the tidal mixing areas toward sinks of CO<sub>2</sub> in the stratified regions less influenced by tidal mixing in agreement with recent global modeling studies (Laruelle et al., 2018). Interestingly, in the tidal mixing ecosystems the sources increased from nearshore to offshore waters, whereas in stratified ecosystems the sink increased toward nearshore waters. Andersson and Mackenzie (2004) first suggested that shelves may have turned from a CO<sub>2</sub> source in the preindustrial time to a sink at present and that the CO<sub>2</sub> uptake rate would increase with time. More recently Cai (2011) and Bauer et al. (2013) suggested an increasing global shelf CO<sub>2</sub> sink with time as a result of the atmospheric pCO<sub>2</sub> increase. The latest SOCAT data confirm this trend with a slower pCO<sub>2</sub> increase in shelf waters compared to atmospheric pCO<sub>2</sub> that could increase the air-sea gradient and thus the uptake of atmospheric CO<sub>2</sub> in the decades to come, although high spatial variability in air-sea fluxes is to be expected



across shelf regions (Laruelle et al., 2018). This is particularly significant for the sWEC, which is a weak source of CO<sub>2</sub> and could potentially become a sink of CO<sub>2</sub> in the coming decades.

## CONCLUSION

The recent OceanObs 2019 conference highlighted the need for innovative and sustained coastal observatories (Farcy et al., 2019) notably for the study of FCO<sub>2</sub>. In the last decade, the emergence of new high-performance pH and pCO<sub>2</sub> sensors has been extremely valuable for the investigation of OA and FCO<sub>2</sub> (Sastri et al., 2019). Here, the implementation of a cardinal buoy of opportunity equipped with such novel sensors into an existing network of time-series and Ferrybox monitoring programs provided a robust multiple year assessment of FCO<sub>2</sub> and also pH variability in a temperate coastal ecosystem. This is particularly relevant on a socio-economical level since nearshore ecosystems host large stocks of shellfish species sensitive to ongoing ocean acidification. Numerous cardinal buoys are present in the global coastal ocean to direct traffic, particularly along rocky shores with large tidal ranges. These buoys of opportunity can be equipped with meteorological and oceanographic sensors and transmit data daily to the shore, thus providing real-time data for the study of coastal ecosystems under climate change. This network of buoys therefore has significant potential to be exploited for efficient, low cost observation of coastal ecosystems.

## DATA AVAILABILITY STATEMENT

Discrete data are available at: <http://somalit-db.epoc.u-bordeaux1.fr/bdd.php?serie=ST&sm=3> (accessed date 14 August 2020).

## AUTHOR CONTRIBUTIONS

J-PG collected, analyzed, processed and interpreted the data, and wrote the first version of the manuscript. PM provided scientific discussion, new ideas on the interpretation of the results, and contributed to writing the manuscript. TC initiated the collaboration on the Cardinal buoy. TC, CG, ÉM, and MV configured the data acquisition system on the buoy, calibrated and cleaned the sensors, collected data in the field, analyzed discrete samples in the laboratory and processed the data. YB designed the study, led the research, interpreted the data, wrote the manuscript, and managed the project. All authors contributed to the article and approved the submitted version.

## FUNDING

This work was funded by the CNRS through INSU [COAST HE, SOMLIT, project CHANNEL (LEFE/CYBER)] and INEE, by the “Conseil Général du Finistère” (CD29) and by the “Region Bretagne” (program ARED, project Hi-Tech). Part of this work was supported by the JERICO-NEXT project from the European Union’s Horizon 2020 Research and Innovation Program under grant agreement no. 654410. YB is P.I. of the CHANNEL and Hi-Tech projects and associate researcher (CRCN) at CNRS. J-PG holds a Ph.D. grant from the Region Bretagne and Sorbonne University (ED129).

## REFERENCES

- Alpine, A. E., and Cloern, J. E. (1985). Differences in *in vivo* fluorescence yield between three phytoplankton size classes. *J. Plankton Res.* 7, 381–390. doi: 10.1093/plankt/7.3.381
- Aminot, A., and Kérouel, R. (2007). *Dosage Automatique des Nutriments dans les Eaux Marines: Méthodes en Flux Continu*. Brest: Ifremer.
- Andersson, A. J., and Mackenzie, F. T. (2004). Shallow-water oceans: a source or sink of atmospheric CO<sub>2</sub>? *Front. Ecol. Environ.* 2:348–353.
- Bakker, D. C., Pfeil, B., Landa, C. S., Metzl, N., O’Brien, K. M., Olsen, A., et al. (2016). A multi-decade record of high-quality fCO<sub>2</sub> data in version 3 of the Surface Ocean CO<sub>2</sub> Atlas (SOCAT). *Earth Syst. Sci. Data* 8, 383–413.
- Bauer, J. E., Cai, W. J., Raymond, P. A., Bianchi, T. S., Hopkinson, C. S., and Regnier, P. A. (2013). The changing carbon cycle of the coastal ocean. *Nature* 504, 61–70. doi: 10.1038/nature12857
- Beucher, C., Treguer, P., Corvaisier, R., Hapette, A. M., and Elskens, M. (2004). Production and dissolution of biosilica, and changing microphytoplankton dominance in the Bay of Brest (France). *Mar. Ecol. Prog. Ser.* 267, 57–69. doi: 10.3354/meps267057
- Bordeyne, F., Migné, A., and Davault, D. (2017). Variation of fucoid community metabolism during the tidal cycle: insights from *in situ* measurements of seasonal carbon fluxes during emersion and immersion. *Limnol. Oceanogr.* 62, 2418–2430. doi: 10.1002/lno.10574
- Borges, A. V., Alin, S. R., Chavez, F. P., Vlahos, P., Johnson, K. S., Holt, J. T., et al. (2010). “A global sea surface carbon observing system: inorganic and organic carbon dynamics in coastal oceans” in *Proceedings of OceanObs’09: Sustained Ocean Observations and Information for Society*, Vol. 2, (Paris: European Space Agency), 67–88. doi: 10.5270/OceanObs09.cwp.07
- Borges, A. V., and Frankignoulle, M. (2003). Distribution of surface carbon dioxide and air sea exchange in the English Channel and adjacent areas. *J. Geophys. Res. Oceans* 108:3140. doi: 10.1029/2000JC000571
- Borges, A. V., and Gypens, N. (2010). Carbonate chemistry in the coastal zone responds more strongly to eutrophication than ocean acidification. *Limnol. Oceanogr.* 55, 346–353.

## ACKNOWLEDGMENTS

We thank the “Service des Phares et Balises” for providing access to the ASTAN buoy and the “Service Mer” of the SBR for their valuable support during sampling at sea. We thank the SNAPOCO<sub>2</sub> for DIC/TA analysis and M. Ramonet for providing the atmospheric CO<sub>2</sub> data from the RAMCES network (Observatory Network for Greenhouse gases). G. Charia (Ifremer) provided valuable help with the wavelet frequency analysis. We thank the SOMLIT (Service d’Observation du Milieu Littoral) network for providing oceanographic data at the SOMLIT sites and help during fieldwork. We thank A. Durand and E. Collin for their help during field campaign on the Penzé river. We are grateful to the Menden-Deuer lab (URI-GSO) and A. C. Baudoux for constructive collaboration and scientific discussions during finalization of the manuscript. We thank I. Probert for correcting the revised manuscript and the two reviewers whose comments greatly improved the quality of the manuscript. In memory of FB.

## SUPPLEMENTARY MATERIAL

The Supplementary Material for this article can be found online at: <https://www.frontiersin.org/articles/10.3389/fmars.2020.00712/full#supplementary-material>

- Bourgeois, T., Orr, J. C., Resplandy, L., Terhaar, J., Ethé, C., Gehlen, M., et al. (2016). Coastal-ocean uptake of anthropogenic carbon. *Biogeosciences* 13, 4167–4185. doi: 10.5194/bg-13-4167-2016
- Bozec, Y., Cariou, T., Macé, E., Morin, P., Thuillier, D., and Vernet, M. (2012). Seasonal dynamics of air-sea CO<sub>2</sub> fluxes in the inner and outer Loire estuary (NW Europe). *Estuar. Coast. Shelf Sci.* 100, 58–71.
- Bozec, Y., Merlivat, L., Baudoux, A. C., Beaumont, L., Blain, S., Bucciarelli, E., et al. (2011). Diurnal to inter-annual dynamics of pCO<sub>2</sub> recorded by a CARIOCA sensor in a temperate coastal ecosystem (2003–2009). *Mar. Chem.* 126, 13–26. doi: 10.1016/j.marchem.2011.03.003
- Bricaud, A., Babin, M., Morel, A., and Claustre, H. (1995). Variability in the chlorophyll-specific absorption coefficients of natural phytoplankton: analysis and parameterization. *J. Geophys. Res. Oceans* 100, 13321–13332. doi: 10.1029/95JC00463
- Bricaud, A., Morel, A., and Prieur, L. (1983). Optical efficiency factors of some phytoplankters 1. *Limnol. Oceanogr.* 28, 816–832. doi: 10.4319/lno.1983.28.5.0816
- Brodeur, J. R., Chen, B., Su, J., Xu, Y. Y., Hussain, N., Scaboo, K. M., et al. (2019). Chesapeake Bay inorganic carbon: spatial distribution and seasonal variability. *Front. Mar. Sci.* 6:99. doi: 10.3389/fmars.2019.00099
- Cai, W.-J. (2011). Estuarine and coastal ocean carbon paradox: CO<sub>2</sub> sinks or sites of terrestrial carbon incineration? *Annu. Rev. Mar. Sci.* 3, 123–145.
- Cai, W. J., Hu, X., Huang, W. J., Murrell, M. C., Lehrter, J. C., Lohrenz, S. E., et al. (2011). Acidification of subsurface coastal waters enhanced by eutrophication. *Nat. Geosci.* 4, 766–770. doi: 10.1038/ngeo1297
- Cai, W.-J., Huang, W.-J., Luther, G. W., Pierrot, D., Li, M., Testa, J., et al. (2017). Redox reactions and weak buffering capacity lead to acidification in the Chesapeake Bay. *Nat. Commun.* 8:369. doi: 10.1038/s-017-00417-7
- Cai, W. J., Wiebe, W. J., Wang, Y., and Sheldon, J. E. (2000). Intertidal marsh as a source of dissolved inorganic carbon and a sink of nitrate in the Satilla River-estuarine complex in the southeastern US. *Limnol. Oceanogr.* 45, 1743–1752. doi: 10.4319/lno.2000.45.8.1743
- Carberry, L., Roesler, C., and et Drapeau, S. (2019). Correcting in situ chlorophyll fluorescence time-series observations for nonphotochemical quenching and



- tidal variability reveals nonconservative phytoplankton variability in coastal waters. *Limnol. Oceanogr. Methods* 17, 462–473. doi: 10.1002/lom3.10325
- Carpenter, J. H. (1965). The accuracy of the winkler method for dissolved oxygen analysis. *Limnol. Oceanogr.* 10, 135–140.
- Cazelles, B., Chavez, M., Berteaux, D., Ménard, F., Vik, J. O., Jenouvrier, S., et al. (2008). Wavelet analysis of ecological time series. *Oecologia* 156, 287–304. doi: 10.1007/s00442-008-0993-2
- Chan, F., Barth, J. A., Blanchette, C. A., Byrne, R. H., Chavez, F., Cheriton, O., et al. (2017). Persistent spatial structuring of coastal ocean acidification in the California Current System. *Sci. Rep.* 7:2526. doi: 10.1038/s41598-017-02777-y
- Chen, C. T. A., and Borges, A. V. (2009). Reconciling opposing views on carbon cycling in the coastal ocean: continental shelves as sinks and near-shore ecosystems as sources of atmospheric CO<sub>2</sub>. *Deep Sea Res. Part II Top. Stud. Oceanogr.* 56, 578–590.
- Chierici, M., Fransson, A., and Anderson, L. G. (1999). Influence of m-cresol purple indicator additions on the pH of seawater samples: correction factors evaluated from a chemical speciation model. *Mar. Chem.* 65, 281–290. doi: 10.1016/S0304-4203(99)00020-1
- Ciais, P., Sabine, C., Bala, G., Bopp, L., Brovkin, V., Canadell, J., et al. (2014). “Carbon and other biogeochemical cycles,” in *Climate change 2013: the physical science basis. Contribution of Working Group I to the Fifth Assessment Report of the Intergovernmental Panel on Climate Change*, eds T. F. Stocker, D. Qin, G.-K. Plattner, M. Tignor, S. K. Allen, et al. (Cambridge: Cambridge University Press), 465–570.
- Clayton, T. D., and Byrne, R. H. (1993). Spectrophotometric seawater pH measurements: total hydrogen ion concentration scale calibration of m-cresol purple and at-sea results. *Deep Sea Res. Part I Oceanogr. Res. Pap.* 40, 2115–2129. doi: 10.1016/0967-0637(93)90048-8
- Cullison Gray, S. E., DeGrandpre, M. D., Moore, T. S., Martz, T. R., Friederich, G. E., and Johnson, K. S. (2011). Applications of in situ pH measurements for inorganic carbon calculations. *Mar. Chem.* 125, 82–90. doi: 10.1016/j.marchem.2011.02.005
- Dai, M., Lu, Z., Zhai, W., Chen, B., Cao, Z., Zhou, K., et al. (2009). Diurnal variations of surface seawater pCO<sub>2</sub> in contrasting coastal environments. *Limnol. Oceanogr.* 54, 735–745. doi: 10.4319/lo.2009.54.3.0735
- DeGrandpre, M. D., Hammar, T. R., Wallace, D. W., and Wirick, C. D. (1997). Simultaneous mooring-based measurements of seawater CO<sub>2</sub> and O<sub>2</sub> off Cape Hatteras, North Carolina. *Limnol. Oceanogr.* 42, 21–28. doi: 10.4319/lo.1997.42.1.0021
- DeGrandpre, M. D., Hammar, T. R., and Wirick, C. D. (1998). Short-term pCO<sub>2</sub> and O<sub>2</sub> dynamics in California coastal waters. *Deep Sea Res. Part II: Top. Stud. Oceanogr.* 45, 1557–1575. doi: 10.1016/S0967-0645(98)80006-4
- de Haas, H., van Weering, T. C., and de Stigter, H. (2002). Organic carbon in shelf seas: sinks or sources, processes and products. *Cont. Shelf Res.* 22, 691–717. doi: 10.1016/S0278-4343(01)00093-0
- De la Paz, M., Gómez-Parra, A., and Forja, J. (2007). Inorganic carbon dynamic and air-water CO<sub>2</sub> exchange in the Guadalquivir Estuary (SW Iberian Peninsula). *J. Mar. Syst.* 68, 265–277. doi: 10.1016/j.jmarsys.2006.11.011
- Del Amo, Y., Quéguiner, B., Tréguer, P., Breton, H., and Lampert, L. (1997). Impacts of high-nitrate freshwater inputs on macrotidal ecosystems. II. Specific role of the silicic acid pump in the year-round dominance of diatoms in the Bay of Brest (France). *Mar. Ecol. Prog. Ser.* 161, 225–237. doi: 10.3354/meps161225
- Dickson, A. G., and Millero, F. J. (1987). A comparison of the equilibrium constants for the dissociation of carbonic acid in seawater media. *Deep Sea Res. Part A Oceanogr. Res. Pap.* 34, 1733–1743. doi: 10.1016/0198-0149(87)90021-5
- Dickson, A. G., Sabine, C. L., and Christian, J. R. (eds) (2007). *Guide to Best Practices for Ocean CO<sub>2</sub> Measurements*. North Pacific Marine Science Organization, 176. Available online at: [www.nodc.noaa.gov/ocads/oceans/Handbook\\_2007.html](http://www.nodc.noaa.gov/ocads/oceans/Handbook_2007.html) (accessed July 17, 2020).
- DOE (1994). *Handbook of Methods for Analysis of the Various Parameters of the Carbon Dioxide System in Sea Water, Version 2*. Available online at: <https://core.ac.uk/download/pdf/98639593.pdf> doi: 10.2172/10107773 (accessed July 17, 2020).
- Doney, S. C., Fabry, V. J., Feely, R. A., and Kleypas, J. A. (2009). Ocean acidification: the other CO<sub>2</sub> problem. *Annu. Rev. Mar. Sci.* 1, 169–192. doi: 10.1146/annurev.marine.010908.163834
- Dumousseaud, C., Achterberg, E. P., Tyrrell, T., Charalampopoulou, A., Schuster, U., Hartman, M., et al. (2010). Contrasting effects of temperature and winter mixing on the seasonal and inter-annual variability of the carbonate system in the Northeast Atlantic, Ocean. *Biogeosciences* 7, 1481–1492. doi: 10.5194/bg-7-1481-2010
- Dürr, H. H., Meybeck, M., Hartmann, J., Laruelle, G. G., and Roubeix, V. (2011). Global spatial distribution of natural riverine silica inputs to the coastal zone. *Biogeosciences* 8, 597–620. doi: 10.5194/bg-8-597-2011
- Edmond, J. M. (1970). High precision determination of titration alkalinity and total carbon dioxide content of sea water by potentiometric titration. *Deep Sea Res. Oceanogr. Abstr.* 17, 737–750. doi: 10.1016/0011-7471(70)90038-0
- Farcy, P., Durand, D., Charria, G., Painting, S. J., Collingridge, K., Grémare, A. J., et al. (2019). Towards a European Coastal Observing Network to provide better answer to science and to societal challenges; the JERICO/JERICO-NEXT Research Infrastructure. *Front. Mar. Sci.* 6:529. doi: 10.3389/fmars.2019.00529
- Feely, R. A., Alin, S., Carter, B., Bednaršek, N., Hales, B., Chan, F., et al. (2016). Chemical and biological impacts of ocean acidification along the west coast of North America. *Estuar. Coast. Shelf Sci.* 183, 260–270. doi: 10.1016/j.ecss.2016.08.043
- Feely, R. A., Alin, S. R., Newton, J., Sabine, C. L., Warner, M., Devol, A., et al. (2010). The combined effects of ocean acidification, mixing, and respiration on pH and carbonate saturation in an urbanized estuary. *Estuar. Coast. Shelf Sci.* 88, 442–449. doi: 10.1016/j.ecss.2010.05.004
- Fennel, K., Alin, S., Barbero, L., Evans, W., Bourgeois, T., Cooley, S., et al. (2019). Carbon cycling in the North American coastal ocean: a synthesis. *Biogeosciences* 16, 1281–1304.
- Forja, J. M., Ortega, T., DelValls, T. A., and Gómez-Parra, A. (2004). Benthic fluxes of inorganic carbon in shallow coastal ecosystems of the Iberian Peninsula. *Mar. Chem.* 85, 141–156. doi: 10.1016/j.marchem.2003.09.007
- Friedlingstein, P., Jones, M., O’sullivan, M., Andrew, R., Hauck, J., Peters, G., et al. (2019). Global carbon budget 2019. *Earth Syst. Sci. Data* 11, 1783–1838. doi: 10.5194/essd-11-1783-2019
- Gattuso, J. P., Frankignoulle, M., and Wollast, R. (1998). Carbon and carbonate metabolism in coastal aquatic ecosystems. *Annu. Rev. Ecol. Syst.* 29, 405–434. doi: 10.1146/annurev.ecolsys.29.1.405
- Goring, D. G., and Bell, R. G. (1999). El Niño and decadal effects on sea-level variability in northern New Zealand: a wavelet analysis. *N. Z. J. Mar. Freshw. Res.* 33, 587–598. doi: 10.1080/00288330.1999.9516902
- Gran, G. (1952). Determination of the equivalence point in potentiometric titrations. Part II. *Analyst* 77, 661–671.
- Grinsted, A., Moore, J. C., and Jevrejeva, S. (2004). Application of the cross wavelet transform and wavelet coherence to geophysical time series. *Nonlinear Process. Geophys.* 11, 561–566.
- Gruber, N., Clement, D., Carter, B. R., Feely, R. A., Van Heuven, S., Hoppema, M., et al. (2019). The oceanic sink for anthropogenic CO<sub>2</sub> from 1994 to 2007. *Science* 363, 1193–1199. doi: 10.1126/science.aau5153
- Guilloux, L., Rigaut-Jalabert, F., Jouenne, F., Ristori, S., Viprey, M., Not, F., et al. (2013). An annotated checklist of Marine Phytoplankton taxa at the SOMLIT-Astan time series off Roscoff (Western English Channel, France): data collected from 2000 to 2010. *Cah. Biol. Mar.* 54, 247–256.
- Hammond, D. E., Giordani, P., Berelson, W. M., and Poletti, R. (1999). Diagenesis of carbon and nutrients and benthic exchange in sediments of the Northern Adriatic Sea. *Mar. Chem.* 66, 53–79. doi: 10.1016/S0304-4203(99)00024-9
- Haraldsson, C., Anderson, L. G., Hasselöv, M., Hulth, S., and Olsson, K. (1997). Rapid, high-precision potentiometric titration of alkalinity in ocean and sediment pore waters. *Deep Sea Res. Part I Oceanogr. Res. Pap.* 44, 2031–2044. doi: 10.1016/S0967-0637(97)00088-5
- Hartman, S. E., Humphreys, M. P., Kivimäe, C., Woodward, E. M. S., Kitidis, V., McGrath, T., et al. (2019). Seasonality and spatial heterogeneity of the surface ocean carbonate system in the northwest European continental shelf. *Prog. Oceanogr.* 177:101909. doi: 10.1016/j.pocean.2018.02.005
- Hofmann, G. E., Smith, J. E., Johnson, K. S., Send, U., Levin, L. A., Micheli, F., et al. (2011). High-frequency dynamics of ocean pH: a multi-ecosystem comparison. *PLoS One* 6:e28983. doi: 10.1371/journal.pone.0028983
- Horwitz, R. M., Hay, A. E., Burt, W. J., Cheel, R. A., Salisbury, J., and Thomas, H. (2019). High-frequency variability of CO<sub>2</sub> in Grand Passage, Bay of Fundy, Nova Scotia. *Biogeosciences* 16, 605–616.



- Hydes, D. J., Hartman, S. E., Hartman, M. C., Jiang, Z., Hardman-Mountford, N., Artioli, Y., et al. (2011). *DEFRApH, Tech. rep. DEFRA Contract ME4133 "DEFRApH Monitoring Project"*. Southampton: National Oceanography Centre Southampton, 53.
- Kapsenberg, L., Alliouane, S., Gazeau, F., Mousseau, L., and Gattuso, J.-P. (2017). Coastal ocean acidification and increasing total alkalinity in the northwestern Mediterranean Sea. *Ocean Sci.* 13, 411–426. doi: 10.5194/os-13-411-2017
- Kapsenberg, L., Miglioli, A., Bitter, M. C., Tambutté, E., Dumollard, R., and Gattuso, J. P. (2018). Ocean pH fluctuations affect mussel larvae at key developmental transitions. *Proc. R. Soc. B* 285:20182381. doi: 10.1098/rspb.2018.2381
- Kitidis, V., Brown, I., Hardman-Mountford, N., and Lefèvre, N. (2017). Surface ocean carbon dioxide during the Atlantic Meridional Transect (1995–2013): evidence of ocean acidification. *Prog. Oceanogr.* 158, 65–75. doi: 10.1016/j.pcean.2016.08.005
- Kitidis, V., Hardman-Mountford, N. J., Litt, E., Brown, I., Cummings, D., Hartman, S., et al. (2012). Seasonal dynamics of the carbonate system in the Western English Channel. *Cont. Shelf Res.* 42, 30–40. doi: 10.1016/j.csr.2012.04.012
- Kitidis, V., Shutler, J. D., Ashton, I., Warren, M., Brown, I., Findlay, H., et al. (2019). Winter weather controls net influx of atmospheric CO<sub>2</sub> on the north-west European shelf. *Sci. Rep.* 9:20153. doi: 10.1038/s41598-019-56363-5
- Laruelle, G. G., Cai, W. J., Hu, X., Gruber, N., Mackenzie, F. T., and Regnier, P. (2018). Continental shelves as a variable but increasing global sink for atmospheric carbon dioxide. *Nat. Commun.* 9:454. doi: 10.1038/s41467-017-02738-z
- Legrand, E., Riera, P., Lutier, M., Coudret, J., Grall, J., and Martin, S. (2017). Species interactions can shift the response of a maerl bed community to ocean acidification and warming. *Biogeosciences* 14, 5359–5376. doi: 10.5194/bg-14-5359-2017
- L'Helguen, S., Madec, C., and Le Corre, P. (1996). Nitrogen uptake in permanently well-mixed temperate coastal waters. *Estuar. Coast. Shelf Sci.* 42, 803–818. doi: 10.1006/ecss.1996.0051
- Litt, E. J., Hardman-Mountford, N. J., Blackford, J. C., Mitchelson-Jacob, G., Goodman, A., Moore, G. F., et al. (2010). Biological control of pCO<sub>2</sub> at station L4 in the Western English Channel over 3 years. *J. Plankton Res.* 32, 621–629. doi: 10.1093/plankt/fbp133
- Liu, Q., Dong, X., Chen, J., Guo, X., Zhang, Z., Xu, Y., et al. (2019). Diurnal to interannual variability of sea surface pCO<sub>2</sub> and its controls in a turbid tidal-driven nearshore system in the vicinity of the East China Sea based on buoy observations. *Mar. Chem.* 216:103690. doi: 10.1016/j.marchem.2019.103690
- Marrec, P. (2014). *Dynamics of the Carbonate System and Air-Sea CO<sub>2</sub> Fluxes in Western European Shelf Waters: A Multi-Scale Approach*. Paris: Sorbonne Université.
- Marrec, P., Cariou, T., Collin, E., Durand, A., Latimier, M., Macé, E., et al. (2013). Seasonal and latitudinal variability of the CO<sub>2</sub> system in the western English Channel based on Voluntary Observing Ship (VOS) measurements. *Mar. Chem.* 155, 29–41. doi: 10.1016/j.marchem.2013.05.014
- Marrec, P., Cariou, T., Latimier, M., Macé, E., Morin, P., Vernet, M., et al. (2014). Spatio-temporal dynamics of biogeochemical processes and air-sea CO<sub>2</sub> fluxes in the Western English Channel based on two years of FerryBox deployment. *J. Mar. Syst.* 140, 26–38. doi: 10.1016/j.jmarsys.2014.05.010
- Marrec, P., Cariou, T., Macé, E., Morin, P., Salt, L. A., Vernet, M., et al. (2015). Dynamics of air-sea CO<sub>2</sub> fluxes in the northwestern European shelf based on voluntary observing ship and satellite observations. *Biogeosciences* 12, 5371–5391. doi: 10.5194/bg-12-5371-2015
- McGrath, T., McGovern, E., Cave, R. R., and Kivimäe, C. (2016). The inorganic carbon chemistry in coastal and shelf waters around Ireland. *Estuaries Coasts* 39, 27–39. doi: 10.1007/s12237-015-9950-6
- McGrath, T., McGovern, E., Gregory, C., and Cave, R. R. (2019). Local drivers of the seasonal carbonate cycle across four contrasting coastal systems. *Reg. Stud. Mar. Sci.* 30:100733. doi: 10.1016/j.rsma.2019.100733
- Mehrbach, C., Culbertson, C. H., Hawley, J. E., and Pytkowicz, R. M. (1973). Measurement of the apparent dissociation constants of carbonic acid in seawater at atmospheric pressure 1. *Limnol. Oceanogr.* 18, 897–907. doi: 10.4319/lo.1973.18.6.0897
- Meybeck, M., Dürr, H. H., and Vörösmarty, C. J. (2006). Global coastal segmentation and its river catchment contributors: a new look at land-ocean linkage. *Glob. Biogeochem. Cycles* 20:W07517. doi: 10.1029/2005GB002540
- Millero, F. J. (2007). The marine inorganic carbon cycle. *Chem. Rev.* 107, 308–341. doi: 10.1021/cr0503557
- Muller-Karger, F. E., Varela, R., Thunell, R., Luerssen, R., Hu, C., and Walsh, J. J. (2005). The importance of continental margins in the global carbon cycle. *Geophys. Res. Lett.* 32:L01602.
- Noisette, F., Bordeyne, F., Davoult, D., and Martin, S. (2016). Assessing the physiological responses of *Crepidula fornicata* to predicted ocean acidification and warming conditions. *Limnol. Oceanogr.* 61, 430–444. doi: 10.1002/lno.10225
- Northcott, D., Sevadjan, J., Sancho-Gallegos, D. A., Wahl, C., Friederich, J., and Chavez, F. P. (2019). Impacts of urban carbon dioxide emissions on sea-air flux and ocean acidification in nearshore waters. *PLoS One* 14:e0214403. doi: 10.1371/journal.pone.0214403
- Oliveira, A. P., Pilar-Fonseca, T., Cabeçadas, G., and Mateus, M. (2018). Local variability of CO<sub>2</sub> partial pressure in a mid-latitude mesotidal estuarine system (Tagus Estuary, Portugal). *Geosciences* 8:460. doi: 10.3390/geosciences8120460
- Orr, J. C., Epitalon, J.-M., Dickson, A., and Gattuso, J.-P. (2018). Routine uncertainty propagation for the marine carbon dioxide system. *Mar. Chem.* 207, 84–107. doi: 10.1016/j.marchem.2018.10.006
- Orr, J. C., Epitalon, J.-M., and Gattuso, J.-P. (2015). Comparison of ten packages that compute ocean carbonate chemistry. *Biogeosciences* 12, 1483–1510. doi: 10.5194/bg-12-1483-2015
- Ostle, C., Williamson, P., Artioli, Y., Bakker, D. C., Birchenough, S. N. R., Davis, C. E., et al. (2016). *Carbon Dioxide and Ocean Acidification Observations in UK Waters: Synthesis Report with a Focus on 2010–2015*. Available online at: [www.researchgate.net/publication/304324178\\_Carbon\\_dioxide\\_and\\_ocean\\_acidification\\_observations\\_in\\_UK\\_waters\\_Synthesis\\_report\\_with\\_a\\_focus\\_on\\_2010\\_-\\_2015?channel=doi&linkId=576be75d08ae4e3add04a1&showFulltext=true](http://www.researchgate.net/publication/304324178_Carbon_dioxide_and_ocean_acidification_observations_in_UK_waters_Synthesis_report_with_a_focus_on_2010_-_2015?channel=doi&linkId=576be75d08ae4e3add04a1&showFulltext=true) (accessed July 17, 2020).
- Ouisse, V., Migné, A., and Davoult, D. (2011). Community-level carbon flux variability over a tidal cycle in *Zostera marina* and *Z. noltii* beds. *Mar. Ecol. Prog. Ser.* 437, 79–87. doi: 10.3354/meps09274
- Padin, X. A., Vázquez-Rodríguez, M., Ríos, A. F., and Pérez, F. F. (2007). Surface CO<sub>2</sub> measurements in the English Channel and Southern Bight of North Sea using voluntary observing ships. *J. Mar. Syst.* 66, 297–308. doi: 10.1016/j.jmarsys.2006.05.011
- Pespeni, M. H., Chan, F., Menge, B. A., and Palumbi, S. R. (2013). Signs of adaptation to local pH conditions across an environmental mosaic in the California Current Ecosystem. *Integr. Comp. Biol.* 53, 857–870. doi: 10.1093/icb/ict094
- Pierrot, D., Wallace, D., Lewis, E., Pierrot, D., Lewis, E., Wallace, R., et al. (2011). *MS Excel Program Developed for CO<sub>2</sub> System Calculations*. Oak Ridge, TN: Oak Ridge National Laboratory. doi: 10.3334/CDIAC/otg.CO2SYS\_XLS\_CDIAC105a
- Pingree, R. D., and Griffiths, D. K. (1978). Tidal fronts on the shelf seas around the British Isles. *J. Geophys. Res. Oceans* 83, 4615–4622. doi: 10.1029/JC083iC09p04615
- Proctor, C. W., and Roesler, C. S. (2010). New insights on obtaining phytoplankton concentration and composition from in situ multispectral Chlorophyll fluorescence. *Limnol. Oceanogr. Methods* 8, 695–708. doi: 10.4319/lom.2010.8.0695
- Puillat, I., Farcy, P., Durand, D., Karlson, B., Petihakis, G., Seppala, J., et al. (2016). Progress in marine science supported by European joint coastal observation systems: the JERICO-RI research infrastructure. *J. Mar. Syst.* 162, 1–3.
- Reimer, J. J., Cai, W.-J., Xue, L., Vargas, R., Noakes, S., Hu, X., et al. (2017). Time series pCO<sub>2</sub> at a coastal mooring: internal consistency, seasonal cycles, and interannual variability. *Cont. Shelf Res.* 145, 95–108. doi: 10.1016/j.csr.2017.06.022
- Reum, J. C., Alin, S. R., Harvey, C. J., Bednaršek, N., Evans, W., Feely, R. A., et al. (2016). Interpretation and design of ocean acidification experiments in upwelling systems in the context of carbonate chemistry co-variation with temperature and oxygen. *ICES J. Mar. Sci.* 73, 582–595. doi: 10.1093/icesjms/fsu231
- Ribas-Ribas, M., Anfuso, E., Gómez-Parra, A., and Forja, J. M. (2013). Tidal and seasonal carbon and nutrient dynamics of the Guadalquivir estuary and the Bay of Cádiz (SW Iberian Peninsula). *Biogeosciences* 10, 4481–4491. doi: 10.5194/bg-10-4481-2013

- Ribas-Ribas, M., Gómez-Parra, A., and Forja, J. M. (2011). Air-sea CO<sub>2</sub> fluxes in the north-eastern shelf of the Gulf of Cádiz (southwest Iberian Peninsula). *Mar. Chem.* 123, 56–66. doi: 10.1016/j.marchem.2010.09.005
- Roobaert, A., Laruelle, G., Landschützer, P., and Régnier, P. (2018). Uncertainty in the global oceanic CO<sub>2</sub> uptake induced by wind forcing: quantification and spatial analysis. *Biogeosciences* 15, 1701–1720. doi: 10.5194/bg-15-1701-2018
- Roobaert, A., Laruelle, G. G., Landschützer, P., Gruber, N., Chou, L., and Régnier, P. (2019). The spatiotemporal dynamics of the sources and sinks of CO<sub>2</sub> in the global coastal ocean. *Glob. Biogeochem. Cycles* 33, 1693–1714. doi: 10.1029/2019GB006239
- Saderne, V., Fietzek, P., and Herman, P. M. J. (2013). Extreme variations of pCO<sub>2</sub> and pH in a macrophyte meadow of the Baltic Sea in summer: evidence of the effect of photosynthesis and local upwelling. *PLoS One* 8:e62689. doi: 10.1371/journal.pone.0062689
- Salisbury, J., Green, M., Hunt, C., and Campbell, J. (2008). Coastal acidification by rivers: A threat to shellfish? *EOS* 89, 513–528. doi: 10.1029/2008EO500001
- Salisbury, J., Vandemark, D., Hunt, C., Campbell, J., Jonsson, B., Mahadevan, A., et al. (2009). Episodic riverine influence on surface DIC in the coastal Gulf of Maine. *Estuar. Coast. Shelf Sci.* 82, 108–118.
- Salomon, J. C., and Breton, M. (1993). An atlas of long-term currents in the Channel. *Oceanol. Acta* 16, 439–448.
- Salt, L. A., Beaumont, L., Blain, S., Bucciarelli, E., Grosstefan, E., Guillot, A., et al. (2016). The annual and seasonal variability of the carbonate system in the Bay of Brest (Northwest Atlantic Shelf, 2008–2014). *Mar. Chem.* 187, 1–15. doi: 10.1016/j.marchem.2016.09.003
- Sanford, E., and Kelly, M. W. (2011). Local adaptation in marine invertebrates. *Annu. Rev. Mar. Sci.* 3, 509–535. doi: 10.1146/annurev-marine-120709-142756
- Santos, C. A. G., and de Moraes, B. S. (2013). Identification of precipitation zones within São Francisco River basin (Brazil) by global wavelet power spectra. *Hydrol. Sci. J.* 58, 789–796. doi: 10.1080/02626667.2013.778412
- Sastri, A., Christian, J. R., Achterberg, E. P., Atamanchuk, D., Buck, J. J. H., Bresnahan, P. J., et al. (2019). Perspectives on in situ sensors for ocean acidification research. *Front. Mar. Sci.* 6:653. doi: 10.3389/fmars.2019.00653
- Shadwick, E. H., Friedrichs, M. A., Najjar, R. G., De Meo, O. A., Friedman, J. R., Da, F., et al. (2019). High-frequency CO<sub>2</sub> system variability over the winter-to-spring transition in a coastal plain estuary. *J. Geophys. Res. Oceans* 124, 7626–7642. doi: 10.1029/2019JC015246
- Sosik, H. M., Chisholm, S. W., and Olson, R. J. (1989). Chlorophyll fluorescence from single cells: interpretation of flow cytometric signals. *Limnol. Oceanogr.* 34, 1749–1761. doi: 10.4319/lo.1989.34.8.1749
- Sosik, H. M., and Mitchell, B. G. (1991). Absorption, fluorescence, and quantum yield for growth in nitrogen-limited *Dunaliella tertiolecta*. *Limnol. Oceanogr.* 36, 910–921. doi: 10.4319/lo.1991.36.5.0910
- Southward, A. J., Langmead, O., Hardman-Mountford, N. J., Aiken, J., Boalch, G. T., Dando, P. R., et al. (2005). Long-term oceanographic and ecological research in the Western English Channel. *Adv. Mar. Biol.* 47, 1–105. doi: 10.1016/s0065-2881(04)7001-1
- Sutton, A. J., Sabine, C. L., Feely, R. A., Cai, W.-J., Cronin, M. F., McPhaden, M. J., et al. (2016). Using present-day observations to detect when anthropogenic change forces surface ocean carbonate chemistry outside preindustrial bounds. *Biogeosciences* 13, 5065–5083. doi: 10.5194/bg-13-5065-2016
- Sutton, A. J., Sabine, C. L., Maenner-Jones, S., Lawrence-Slavas, N., Meinig, C., Feely, R. A., et al. (2014). A high-frequency atmospheric and seawater pCO<sub>2</sub> data set from 14 open ocean sites using a moored autonomous system. *Earth Sys. Sci. Data* 6, 353–366. doi: 10.5194/essd-6-353-2014
- Takahashi, T., Olafsson, J., Goddard, J. G., Chipman, D. W., and Sutherland, S. C. (1993). Seasonal variation of CO<sub>2</sub> and nutrients in the high-latitude surface oceans: a comparative study. *Glob. Biogeochem. Cycles* 7, 843–878. doi: 10.1029/93GB02263
- Takahashi, T., Sutherland, S. C., Sweeney, C., Poisson, A., Metzl, N., Tilbrook, B., et al. (2002). Global sea-air CO<sub>2</sub> flux based on climatological surface ocean pCO<sub>2</sub>, and seasonal biological and temperature effects. *Deep Sea Res. Part II Top. Stud. Oceanogr.* 49, 1601–1622. doi: 10.1016/S0967-0645(02)00003-6
- Thomas, C. D., Cameron, A., Green, R. E., Bakkenes, M., Beaumont, L. J., Collingham, Y. C., et al. (2004). Extinction risk from climate change. *Nature* 427, 145–148. doi: 10.1038/nature02121
- Thomas, H., Bozec, Y., de Baar, H. J., Borges, A., and Schiettecatte, L. S. (2005). Controls of the surface water partial pressure of CO<sub>2</sub> in the North Sea. *Biogeosciences* 2, 323–334. doi: 10.5194/bg-2-323-2005
- Tréguer, P., Goberville, E., Barrier, N., l'Helguen, S., Morin, P., Bozec, Y., et al. (2014). Large and local-scale influences on physical and chemical characteristics of coastal waters of Western Europe during winter. *J. Mar. Syst.* 139, 79–90. doi: 10.1016/j.jmarsys.2014.05.019
- Tréguer, P. J., and De La Rocha, C. L. (2013). The world ocean silica cycle. *Annu. Rev. Mar. Sci.* 5, 477–501. doi: 10.1146/annurev-marine-121211-172346
- Tsunogai, S., Watanabe, S., and Sato, T. (1999). Is there a “continental shelf pump” for the absorption of atmospheric CO<sub>2</sub>? *Tellus B* 51, 701–712. doi: 10.3402/tellusb.v51i3.16468
- Vargas, C. A., Lagos, N. A., Lardies, M. A., Duarte, C., Manríquez, P. H., Aguilera, V. M., et al. (2017). Species-specific responses to ocean acidification should account for local adaptation and adaptive plasticity. *Nat. Ecol. Evol.* 1:0084. doi: 10.1038/s41559-017-0084
- Wafar, M. V. M., Le Corre, P., and Birrien, J. L. (1983). Nutrients and primary production in permanently well-mixed temperate coastal waters. *Estuar. Coast. Shelf Sci.* 17, 431–446. doi: 10.1016/0272-7714(83)90128-2
- Waldbusser, G. G., and Salisbury, J. E. (2014). Ocean acidification in the coastal zone from an organism's perspective: multiple system parameters, frequency domains, and habitats. *Annu. Rev. Mar. Sci.* 6, 221–247. doi: 10.1146/annurev-marine-121211-172238
- Walsh, J. J. (1991). Importance of continental margins in the marine biogeochemical cycling of carbon and nitrogen. *Nature* 350, 53–55. doi: 10.1038/350053a0
- Walsh, J. J., Biscaye, P. E., and Csanady, G. T. (1988). The 1983–1984 shelf edge exchange processes (SEEP)—I experiment: hypotheses and highlights. *Cont. Shelf Res.* 8, 435–456. doi: 10.1016/0278-4343(88)90063-5
- Wanninkhof, R. (2014). Relationship between wind speed and gas exchange over the ocean revisited. *Limnol. Oceanogr. Methods* 12, 351–362. doi: 10.4319/lom.2014.12.351
- Wanninkhof, R., Asher, W. E., Ho, D. T., Sweeney, C., and McGillis, W. R. (2009). Advances in quantifying air-sea gas exchanges and environmental forcings. *Annu. Rev. Mar. Sci.* 1, 213–244. doi: 10.1146/annurev.marine.010908.163742
- Weiss, R. F. (1970). The solubility of nitrogen, oxygen and argon in water and seawater. *Deep Sea Res. Oceanogr. Abstr.* 17, 721–735. doi: 10.1016/0011-7471(70)90037-9
- Weiss, R. F., and Price, B. A. (1980). Nitrous oxide solubility in water and seawater. *Mar. Chem.* 8, 347–359. doi: 10.1016/0304-4203(80)90024-9
- Wimart-Rousseau, C., Lajaunie-Salla, K., Marrec, P., Wagener, T., Raimbault, P., Lagadec, V., et al. (2020). Temporal variability of the carbonate system and air-sea CO<sub>2</sub> exchanges in a Mediterranean human-impacted coastal site. *Estuar. Coast. Shelf Sci.* 236:106641. doi: 10.1016/j.ecss.2020.106641
- Xing, X., Claustre, H., Blain, S., d'Ortenzio, F., Antoine, D., Ras, J., et al. (2012). Quenching correction for in vivo chlorophyll fluorescence acquired by autonomous platforms: a case study with instrumented elephant seals in the Kerguelen region (Southern Ocean). *Limnol. Oceanogr. Methods* 10, 483–495. doi: 10.4319/lom.2012.10.483
- Xue, L., Cai, W.-J., Hu, X., Sabine, C., Jones, S., Sutton, A. J., et al. (2016). Sea surface carbon dioxide at the Georgia time series site (2006–2007): air-sea flux and controlling processes. *Prog. Oceanogr.* 140, 14–26. doi: 10.1016/j.pocean.2015.09.008
- Yang, M., Bell, T. G., Brown, I. J., Fishwick, J., Kitidis, V., Nightingale, P. D., et al. (2019). Insights from year-long measurements of air-water CH<sub>4</sub> and CO<sub>2</sub> exchange in a coastal environment. *Biogeosciences* 16, 961–978. doi: 10.5194/bg-16-961-2019
- Zeebe, R. E., and Wolf-Gladrow, D. (2001). *CO<sub>2</sub> in Seawater: Equilibrium, Kinetics, Isotopes* (No. 65). Houston, TX: Gulf Professional Publishing.

**Conflict of Interest:** The authors declare that the research was conducted in the absence of any commercial or financial relationships that could be construed as a potential conflict of interest.

Copyright © 2020 Gac, Marrec, Cariou, Guillermin, Macé, Vernet and Bozec. This is an open-access article distributed under the terms of the Creative Commons Attribution License (CC BY). The use, distribution or reproduction in other forums is permitted, provided the original author(s) and the copyright owner(s) are credited and that the original publication in this journal is cited, in accordance with accepted academic practice. No use, distribution or reproduction is permitted which does not comply with these terms.